Synergistic Mechanisms of Green Equisetum-Synthesized Silica Nanocomposite, Gemini Surfactant and Low Salinity Water from Interfacial Modifications to Spontaneous Imbibition Driven Enhanced Oil Recovery

Ali Yarahmadi
Petroleum University of Technology
Ghasem Zargar
ghasemzargar59@gmail.com

Petroleum University of Technology
Siavash Ashoori
Petroleum University of Technology
Abbas Khaksar Manshad
Petroleum University of Technology (PUT)

Article

Keywords: Enhanced Oil Recovery, Gemini Surfactants, Green Nanocomposite, Wettability Alteration, Interfacial Tension Reduction

Posted Date: October 16th, 2025

DOI: https://doi.org/10.21203/rs.3.rs-7697137/v1

Additional Declarations: No competing interests reported.

Version of Record: A version of this preprint was published at Scientific Reports on January 3rd, 2026.
See the published version at https://doi.org/10.1038/s41598-025-34465-7.

Synergistic Mechanisms of Green *Equisetum*-Synthesized Silica Nanocomposite, Gemini Surfactant and Low Salinity Water from Interfacial Modifications to Spontaneous Imbibition Driven Enhanced Oil Recovery

Ali Yarahmadi[1], Ghasem Zargar[1*](Corresponding Author), Siavash Ashoori[1], Abbas Khaksar Manshad[2]

Corresponding Author Email: ghasemzargar59@gmail.com

[1] Department of Petroleum Engineering, Ahwaz Faculty of Petroleum Engineering, Petroleum University of Technology, Ahwaz, Iran

[2] Department of Petroleum Engineering, Abadan Faculty of Petroleum Engineering, Petroleum University of Technology (PUT), Abadan, Iran

1- Abstract

Developing environmentally benign yet high-performance enhanced oil recovery (EOR) strategies for carbonate reservoirs remains a pressing challenge due to their oil-wet nature and complex brine chemistry. In this study, we introduce a mechanistically designed ternary system comprising plant-derived *Equisetum arvense* nanosilica (NS), a novel cationic Gemini surfactant (T14S3), and sulfate-enriched low-salinity brine (Na_2SO_4) to achieve multi-scale interfacial control. Comprehensive physicochemical analyses confirmed the amorphous, silanol-rich morphology of the nanosilica and the bis-quaternary architecture of T14S3, exhibiting complementary electrostatic tendencies. Zeta potential measurements revealed tunable surface charge from ≈ –70 mV to +30 mV via sulfate-mediated adsorption and double-layer compression. The ternary formulation achieved ultralow interfacial tension (IFT) (0.51 mN/m at 5500 ppm Na_2SO_4) and pronounced wettability alteration (contact angle reduction from ≈ 138° to 34° at 2000 ppm Na_2SO_4). Langmuir modeling confirmed enhanced cooperative adsorption of NS and T14S3 under optimal salinity. Spontaneous imbibition tests demonstrated that the 2000 ppm Na_2SO_4 blend recovered 25.4 % OOIP, more than twice the baseline brine, highlighting wettability alteration as the dominant mechanism once IFT entered the sub 1 mN/m domain. By integrating green

nanomaterials, advanced surfactant architecture, and targeted ionic tuning, this work establishes a low-carbon, scalable framework for sustainable EOR, aligning with circular economy and reservoir management goals.

Keywords: Enhanced Oil Recovery, Gemini Surfactants, Green Nanocomposite, Wettability Alteration, Interfacial Tension Reduction

2- Introduction

The progressive depletion of easy-to-recover hydrocarbon reserves, particularly in carbonate formations, has driven the petroleum industry toward advanced enhanced oil recovery (EOR) strategies capable of operating under harsh reservoir conditions [1, 2]. Carbonate reservoirs, which account for more than half of the world's proven oil reserves, pose unique challenges due to their inherent heterogeneity, low permeability, and predominantly oil-wet wettability [3]. Recent industrial and environmental demands emphasize the need for "green" and sustainable EOR solutions that minimize chemical footprint while maintaining operational efficiency, aligning with circular economy and environmental compliance goals [4].

Plant-derived nanomaterials have recently emerged as attractive EOR agents due to their renewability, low toxicity, and surface tunability [5]. Silica-based nanoparticles, in particular, offer high specific surface areas and abundant Si–OH groups, enabling effective adsorption and wettability alteration on carbonate surfaces [6-8]. As summarized in Table 1, multiple studies have demonstrated their ability to stabilize emulsions, reduce interfacial tension, and improve oil displacement efficiency, especially when synthesized from biogenic sources [9]. However, most prior works have tested these particles either in isolation or under simplified saline conditions, without fully addressing salinity tolerance and long-term stability in realistic carbonate brines.

Table 1. Representative studies on green nanocomposites for EOR

Reference	Year	NCs type and Source	Key Finding Related to EOR
Nazarahari et al. [10]	2020	CeO_2@Nanoclay - *Capsicum frutescent* leaves	At 500 ppm, reduced IFT from 35 mN/m to 17 mN/m (48.5%) and altered carbonate contact angle from 139° to 53° (38% improvement); high thermal stability up to 90 °C; zeta potential peak indicated stable nanofluid.
AK.Manshad [11]	2022	ZnO/SiO_2@Nanoclay — green synthesis using *Cordyline fruticosa* extract	2000 ppm in distilled water reduced IFT and contact angle to 65.5°; achieved 62.14 % OOIP in secondary recovery and improved tertiary recovery from 44 % to 65.41 % OOIP.
A.Jagar et al. [12]	2021	TiO_2/SiO_2/poly(acrylamide) NCs — green synthesis using pomegranate seed extract	1500 ppm NCs with 5000 ppm $CaSO_4$ + $CaCl_2$ reduced IFT by 65% and altered wettability by 32%; increased oil recovery from 36.0 % to 46.53 % OOIP in carbonate cores.
Nourinia et al. [13]	2022	ZnO/montmorillonite (MMT) NCs — combined with natural saponin from *Cyclamen persicum*	At optimum concentration, hybrid CP–ZnO/MMT nanofluid reduced IFT by 57.78 % and contact angle by 61.58 %; improved oil recovery factor by 13 % in carbonate cores compared to baseline.
Bahraminejad et al. [14]	2019	CuO/TiO_2/PAM NCs — green synthesis using *Cassytha filiformis L.* fruit extract	At 200 ppm, reduced IFT by ~46 % and altered carbonate wettability by 90 % (151°→14.7°); in sandstone, optimum 1500 ppm achieved 91 % wettability shift (135.25°→11.75°).
Omidi et al [15]	2020	Fe_3O_4@eggshell NC — green synthesis using *Commersonia bartramia* extract	500 ppm NC + 1000 ppm CTAB hybrid reduced IFT to 0.18 mN/m and CA to 60.7°, improving oil recovery by 8.16% OOIP (47%→55.15%) from carbonate cores.

Zarger et al [16]	2020	TiO_2/Quartz NC — green synthesis using *Euphoria condylocarpa* extract	1000 ppm in distilled water reduced IFT from 36.4→3.5 mN/m and CA from 103°→48°, enabling 21% OOIP additional recovery in carbonate cores.
Nazarahari et al [17]	2021	Adinandra Dumosa plant	At optimal 250 ppm (carbonate cores) reduced IFT by 56% (36→15.42 mN/m), shifted CA from 150°→33°, and increased tertiary oil RF by 11.72%; in sandstone cores at 1000 ppm shifted CA from 140°→34° and increased RF by 15.79%.

Gemini surfactants, characterized by two hydrophobic tails and two polar headgroups linked by a spacer, exhibit significantly lower critical micelle concentrations (CMCs) and higher surface activities than traditional monomeric counterparts [18, 19]. Their dual-binding structure enables robust adsorption at oil–water and rock–water interfaces, facilitating simultaneous interfacial tension reduction and wettability alteration [20]. Table 2 summarizes recent studies employing Gemini surfactants in EOR, where their unique molecular architecture often translates into lower dosages and enhanced thermal and saline stability. Yet, despite promising results, the combined application of Gemini surfactants with green-derived nanoparticles under optimized ionic conditions in carbonate systems remains insufficiently explored.

Table 2. Representative studies on Gemini surfactants for EOR

Reference (Year)	Gemini type & source	Test conditions	IFT & CA change	Oil recovery improvement
Al-Azani *et al.* (2024) [21]	Cationic Gemini surfactant GS8, in-house synthesized	Coreflood in Indiana limestone, 100 °C; brine, brackish water,	n/a	+23% OOIP (brine), +26.3% OOIP (brackish water), +37% OOIP (with

		+DTPA (1 wt%), +methylene blue (300 ppm); 2500 ppm surfactant		DTPA) ultimate RF 84%; low retention (0.35–0.41 mg/g)
Wang *et al.* (2023) [22]	Cationic Gemini 16–4–16 + anionic SDBS mixture (synthetic)	Coreflood; diesel/crude oil systems; salinity 5,000–20,000 mg/L; αSDBS = 0.4; 25 °C	IFT to $<10^{-2}$ mN/m (min 3.3×10^{-3} mN/m); CA from 107° → 46°	+26.2% crude oil recovery
Pal *et al.* (2018) [20]	Cationic Gemini 14-s-14 series (s = 3, 4, 5, 6), synthetic	Sandpack flooding; high salinity; thermal stability; polymer-surfactant formulations	IFT: 10^{-2}–10^{-3} mN/m; CA: intermediate-wet → water-wet	+29.83% (14-3-14), +31.73% (14-4-14), +33.83% (14-5-14), +34.55% (14-6-14)
Hou *et al.* (2019) [23]	Cationic Gemini ANG (synthetic, high T & salinity tolerant)	Coreflood; 120 °C; high salinity (200 g/L TDS, Ca^{2+} = 5000 mg/L)	IFT: min 7.81×10^{-3} mN/m at 120 °C; 8.75×10^{-3} mN/m in high salinity; CA: 135° → 62°	+17.3% OOIP
Mpelwa *et al.* (2019) [24]	Extended Gemini Surfactants (EGS1, synthetic, intermediate polarity group)	Coreflood; 30–60 °C; IFT evaluated with/without salts	IFT: ultralow 10^{-3} mN/m, reduced to 10^{-4} mN/m with salts; CA not specified	+12.30% OOIP
Yuan *et al.* (2017) [25]	Cationic Gemini BA-14 (synthetic)	Coreflood; high salinity (65,430 mg/L); 50 °C	IFT: 10^{-3} mN/m; CA: 98° → 33°	+11.09% OOIP
Ma *et al.* (2019) [26]	Anionic-nonionic Gemini surfactant (synthetic)	Coreflood; Dagang crude oil	IFT: 0.0804 mN/m (600 mg/L); CA:	+7.03% OOIP

			144.5° → 71.5° (1500 mg/L)	
Chen *et al.* (2019) [27]	Anionic Gemini surfactant (AGS), synthetic; mixed with lauryl diethanol amide	Hypersaline; 50–70 °C; salinity 20,000–50,000 mg/L; dosage 500–3000 mg/L	IFT: < 10^{-2} mN/m (Bamianhe crude oil); CA not specified	Not specified
Gu *et al.* (2021) [28]	Sulfate-quaternary ammonium amphoteric Gemini surfactants (C12ZGS, C14ZGS, C16ZGS), synthetic	Simulated low-permeability reservoir; high salinity (up to 50,000 mg/L)	IFT: C12ZGS, C14ZGS → 10^{-2} mN/m; C16ZGS → 10^{-1} mN/m; CA not specified	11.63% (C12ZGS), 10.91% (C14ZGS), 9.87% (C16ZGS)
Dong *et al.* (2014) [29]	Zwitterionic Gemini surfactants with varied hydrophobic tails (synthetic)	Sandstone micro-model flooding	IFT: 0.1–1.0 mN/m; CA: improved wetting (value not specified)	+21–29% displacement efficiency

While both green silica nanocomposites and Gemini surfactants have individually demonstrated strong potential for interfacial property modification and enhanced oil recovery—via mechanisms such as surface charge modulation, interfacial tension reduction, and wettability alteration—their combined use in ternary systems optimized with targeted ionic compositions in low-salinity brines remains scarcely explored [30]. Most prior work has focused on binary systems, neglecting the distinctive cooperative effects arising from the simultaneous presence of nanoparticles, surfactant molecules, and specific ionic species in complex carbonate environments.

In this study, mechanistic interactions among *Equisetum arvense*-derived nanosilica, the Gemini surfactant T14S3, and sulfate-rich low-salinity water are systematically examined. The

investigation progresses from assessing the individual contribution of each component, to evaluating binary combinations, and finally to characterizing the fully integrated ternary formulation. Particular emphasis is placed on identifying whether certain mechanisms dominate, complement, or suppress others, as well as on clarifying the operational benefits conferred under reservoir-relevant conditions.

The key synergistic processes investigated include charge inversion with electrostatic stabilization, minimization of oil–water interfacial tension under optimal sulfate salinity, acceleration of wettability reversal from oil-wet to water-wet, cooperative adsorption enhancing retention at carbonate surfaces, and superior capillary-driven oil recovery. The experimental program spans multiple scales, from electrokinetic and adsorption analyses to dynamic interfacial tension, contact angle monitoring, and spontaneous imbibition tests in carbonate cores, yielding both quantitative performance metrics and a detailed mechanistic map explaining the ternary system's advantages over its binary and single-component counterparts.

3- Material and Methods

3-1 Materials

All chemicals and reagents used in this study were of analytical grade unless otherwise specified, and deionized water (resistivity $\geq 18\ M\Omega \cdot cm$) was used in all preparations. *Equisetum arvense* (horsetail) plant material was purchased from a local herbal store (Attari) in Ahvaz, Iran, and employed for the green synthesis of nanoparticles. Sodium sulfate (Na_2SO_4) (analytical grade, >99% purity, Merck, Germany) was used to adjust brine salinity to predetermined levels in order to evaluate the effects of ionic strength on wettability alteration, interfacial tension, and spontaneous imbibition performance.

The reagents for the synthesis of the Gemini surfactant, including N,N,N′,N′-tetramethylethane-1,n-diamine (n = 2, 3, 4), long-chain 1-bromoalkanes, dry acetone, and diethyl ether, were purchased from Merck and Aldrich chemical companies (Germany, USA) and used as received. A representative crude oil sample was sourced from a producing oilfield in southwest Iran, while natural seawater, collected from the northern coast of the Persian Gulf, served as the base brine. Carbonate outcrop blocks, sourced from formations surrounding a southwestern Iranian oil field, were selected for core preparation. X-ray diffraction (XRD) analysis confirmed that calcite was the dominant mineral phase in these samples. The physical and chemical properties of the formation, sea water (base brine) and crude oil is summarized in Table 3 and 4 respectively.

Table 3. Formation and Sea Water Properties

Salt	Formation Water (FW) (ppm)	Sea Water (SW) (ppm)
K^+/Na^+	75178	12533
Ca^{2+}	9620	451
Mg^{2+}	1455	156
SO_4^{2-}	555	3218
HCO_3^-	483	141
Cl^-	136678	22659
TDS	223969	39154

Table 4. Crude Oil Properties

Density (g/cm^3)	**Viscosity** (cp)	**Acid no.** (mg KOH/g)	**Base no.** (mg HCl/g)	**Asphaltene Content.** (%)
0.882	38	2.46	1.57	2.3

3-2 Synthesis and Preparation of Materials

3-2-1 Synthesis of Gemini Surfactant

The cationic gemini surfactant with two C_{14} hydrophobic tails and a C_3 spacer, hereafter referred to as *T14S3*, was synthesized via a two-step quaternization reaction. Briefly, 0.05 mol of N,N,N′,N′-tetramethylethane-1,3-diamine was dissolved in 20 mL of anhydrous acetone under a nitrogen atmosphere. Subsequently, 0.11 mol of 1-bromotetradecane was added dropwise under constant magnetic stirring. The mixture was refluxed at 70–80 °C for 48 h, with the temperature precisely maintained using a thermocouple probe. After completion, the solvent was removed under reduced pressure using a rotary evaporator. The crude residue was washed thoroughly with cold diethyl ether to remove unreacted reagents and byproducts, then vacuum-dried at 40 °C for 12 h to yield T14S3 as an off-white crystalline powder. Structural confirmation and purity verification were performed using Fourier-transform infrared (FTIR) and proton nuclear magnetic resonance (^{1}H- NMR) spectroscopy. The prepared surfactant was stored in airtight glass vials under inert conditions until further use. A schematic illustration of the synthesis route is provided in Figure 1.

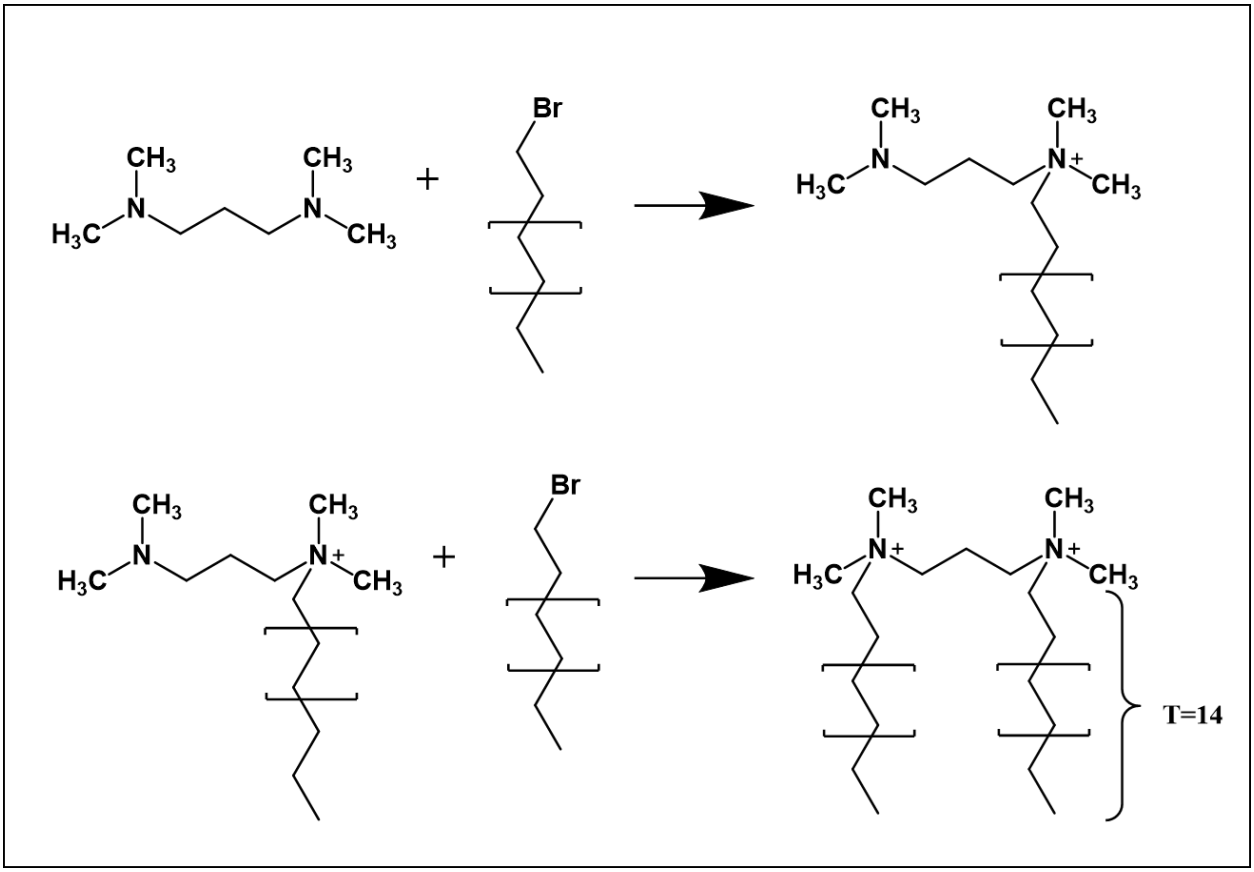

Figure 1. Schematic of T14S3 Gemini Surfactant Synthesis Route.

3-2-2 Preparation of Plant-Derived Nanosilica from *Equisetum arvense*

Fresh aerial parts of *Equisetum arvense* were collected from local herbal store (Attari) in Ahvaz, Iran, washed thoroughly with deionized water to remove dirt and soluble contaminants, and shade-dried for 7 days at ambient temperature (~25 °C). The dried biomass was oven-dried at 60 °C for 24 h to remove residual moisture, then milled to a fine powder and sieved through a 250 µm mesh.

Fifty grams of dried plant powder were dispersed in 500 mL deionized water in a 1 L round-bottom flask, fitted with a condenser, and refluxed at 95–100 °C for 4 h. After cooling to room temperature, the solids were separated by filtration (Whatman No. 1) and washed repeatedly with hot deionized water until the filtrate reached near-neutral pH.

The washed plant residue was transferred to 500 mL of 1 M NaOH, heated to 90 °C, and stirred for 2 h to dissolve the silica as sodium silicate. The hot mixture was filtered to remove insoluble residues. Silica was precipitated from the filtrate by gradual titration with 1 M HCl under constant stirring until pH ≈ 7. The resulting amorphous silica precipitate was aged for 12 h in the mother liquor to improve particle integrity.

The precipitated silica was separated by centrifugation at 5000 rpm for 15 min, washed three times with deionized water to remove salts, and oven-dried at 60 °C for 24 h. The dried cake was gently ground in an agate mortar to a fine, free-flowing nanosilica powder and stored in airtight amber bottles under desiccation until further use in fluid formulations.

3-3 Characterization Techniques

3-3-1 X-ray Diffraction (XRD)

- *Reservoir Carbonate Core.*

The mineralogical composition of the reservoir core sample, classified as carbonate, was determined by X-ray diffraction. Powdered rock specimens (particle size < 75 μm, obtained using an agate mortar) were analyzed with an XRD instrument (Bruker D8 Advance, Germany) equipped with Cu Kα radiation (λ = 1.5406 Å). Data were collected over a 2θ range of 10°–90° and a scanning rate of 1° min^{-1} under an operating voltage of 40 kV and a current of 40 mA. Phase identification was performed using the PDF-4+ database (International Centre for Diffraction Data, ICDD) in conjunction with the Bruker EVA software package.

- *Green Equisetum-Derived Nanosilica.*

XRD analysis was also employed to examine the crystalline/amorphous nature of the nanosilica synthesized via green extraction from *Equisetum arvense*. The dried nanosilica powder was

subjected to XRD under the same instrumental parameters as for the carbonate core. The acquired diffraction profiles were used to confirm the siliceous framework and to assess the degree of amorphicity, which is critical for evaluating surface reactivity and potential interactions with reservoir fluids in subsequent enhanced oil recovery (EOR) applications.

3-3-2 Fourier Transform Infrared Spectroscopy (FTIR)

The chemical structure and functional groups of the raw materials, plant-derived nanosilica (NS), and the synthesized Gemini surfactant (GS), were examined using Fourier transform infrared spectroscopy. Dried powder samples were homogenously mixed with spectroscopic-grade KBr and compressed into transparent pellets under a pressure of 10 MPa. FTIR spectra were recorded in the range of **4000–500 cm^{-1}** with a spectral resolution of **4 cm^{-1}** using a high-sensitivity infrared spectrometer (PerkinElmer Spectrum Two, USA), averaging **32 scans** to enhance the signal-to-noise ratio.

The collected spectra were later analyzed to identify characteristic vibrational modes corresponding to siloxane, and quaternary ammonium structures, which are discussed in detail in the Results and Discussion section.

3-3-3 Proton Nuclear Magnetic Resonance (^{1}H NMR)

Proton nuclear magnetic resonance spectroscopy was employed to confirm the molecular structure of the synthesized Gemini surfactant (GS). Measurements were performed using a high-field NMR spectrometer (Bruker Avance III HD, 400 MHz) equipped with a 5 mm broadband probe. Approximately 10 mg of purified GS was dissolved in 0.7 mL of deuterated chloroform ($CDCl_3$, ≥99.8 atom % D, containing 0.03% v/v tetramethylsilane [TMS] as an internal reference). The solution was transferred into standard NMR tubes and degassed prior to analysis. Spectra were

acquired at 298 K, with an acquisition time of 4.0 s, a relaxation delay of 1.0 s, and 64 scans to ensure an adequate signal-to-noise ratio. Spectral processing was carried out using Bruker TopSpin software.

In this work, the synthesized nanoparticles are primarily composed of silica (SiO_2) extracted from *Equisetum* plant biomass via calcination. This process removes the majority of the organic matrix, yielding an inorganic amorphous silica network devoid of hydrogen atoms in its lattice. Since proton nuclear magnetic resonance spectroscopy detects resonance signals from hydrogen nuclei within organic moieties, it is inherently unsuitable for structural characterization of pure inorganic silica. Previous studies have similarly reported that ^{1}H NMR provides negligible information for calcined silica nanoparticles due to the absence of proton-containing organic groups in the final product [31].

Therefore, ^{1}H NMR analysis was not conducted, and alternative techniques with higher relevance to inorganic nanomaterials were employed. FTIR spectroscopy was used to verify the presence of silanol groups and confirm siloxane bonding, while XRD was applied to assess the amorphous siliceous structure. These characterization methods have been widely adopted for silica-based nanoparticles in the literature.

The observed chemical shifts and assignments for GS are presented in the **Results and Discussion** section.

3-3-4 Thermogravimetric Analysis (TGA)

Thermogravimetric analysis was conducted to evaluate the thermal stability and decomposition profiles of the synthesized Gemini surfactant (T14S3) and nanosilica samples. Analyses were performed using a TGA/DSC1 analyzer (Mettler Toledo, Switzerland) under nitrogen flow

(50 mL min^{-1}). Approximately 5–10 mg of each dried sample was loaded into a platinum crucible and heated at a constant rate of 10 °C min^{-1} from ambient temperature up to a maximum of 300 °C for the organic surfactant, and up to 700 °C for the silica-based samples. The lower terminal temperature for the surfactant ensured complete characterization of its decomposition within the organic stability range, whereas the extended range for nanosilica allowed for detection of residual biogenic organics and assessment of its high-temperature structural stability.

3-3-5 Zeta Potential Analysis

Zeta potential measurements were performed using a Malvern Zetasizer Nano ZS (Malvern Panalytical Ltd., UK) equipped with an automatic titration unit to cover a pH range of 4–12. Five experimental systems were evaluated: (i) carbonate rock powder; (ii) nanosilica derived from Equisetum arvense biomass; (iii) carbonate rock powder with Gemini surfactant T14S3; (iv) carbonate rock powder with plant-based nanosilica; and (v) carbonate rock powder in the presence of Na_2SO_4. For each run, the solid fraction was dispersed in deionized water or the designated electrolyte using a calibrated magnetic stirrer for 15 min, followed by probe ultrasonication at 40 kHz and 120 W for 10 min in an ice bath to minimize thermal effects. The suspensions were equilibrated at 25 ± 1 °C before measurement. pH adjustments were made using 0.1 M HCl or NaOH, and all measurements were conducted in triplicate for reproducibility.

3-3-6 Dynamic Light Scattering (DLS)

The hydrodynamic diameter and particle size distribution of plant-derived nanosilica and Gemini surfactant aggregates were determined using a Malvern Zetasizer Nano ZS (Malvern Panalytical, UK) operating at a backscattering angle of 173 ° and a wavelength of 633 nm. Nanosilica was synthesized via the green protocol described in Section 3-2-2 and stored in airtight vials prior to analysis. For measurements, freshly prepared dispersions of nanosilica in deionized water were

homogenized by magnetic stirring and subsequently sonicated in an ultrasonic bath (40 kHz, 120 W) under ice bath cooling to minimize thermal effects.

Micellar solutions of the Gemini surfactant (T14S3) were prepared in deionized water and equilibrated at 25 ± 0.1 °C before analysis. All DLS measurements were performed in triplicate, with each run consisting of 12 sub-measurements averaged automatically by the instrument software. Particle size distribution data were fitted to both Gaussian and Lorentzian models using OriginPro 2023 (OriginLab, USA) to evaluate peak sharpness and symmetry.

3-3-7 Stability Assessment of Green-Derived Nanosilica Dispersions

The colloidal stability of *Equisetum*-derived nanosilica (NS) dispersions was evaluated by monitoring sedimentation and turbidity retention under conditions relevant to enhanced oil recovery (EOR). Dispersions (0.1 wt% NS) were prepared in four aqueous media, deionized water (DIW), 2000 ppm Na_2SO_4, 5500 ppm Na_2SO_4, and 10 000 ppm Na_2SO_4, as well as in the presence of Gemini surfactant T14S3 (1.5 × CMC) plus 5500 ppm Na_2SO_4.

Each formulation was homogenized by magnetic stirring (400 rpm, 15 min) followed by probe ultrasonication (40 kHz, 120 W, 10 min) in an ice bath to prevent thermal effects. Prepared dispersions were transferred into sealed 20 mL graduated glass vials and placed in thermostated chambers at 25 ± 0.1 °C and 60 ± 0.5 °C.

Two stability indices were monitored over 30 days:

1. **Sedimentation Index (SI)** – At the end of the storage period, the volume ratio of settled material to total dispersion volume was read directly from vial graduations and expressed as a percentage. Lower SI values indicate higher colloidal stability.

2. **Turbidity Retention** – The optical density at 600 nm (OD_{600}) was measured using a UV–Vis spectrophotometer immediately after preparation and after 30 days. Turbidity retention (%) was calculated as: $OD_{600,\ t=30d}$

$$\text{Retention} = \frac{\mathbf{OD}_{600,\ t=30d}}{\mathbf{OD}_{600,\ t=0d}} \times 100 \quad (1)$$

Values close to 100 % signify minimal particle aggregation or sedimentation. All measurements were conducted in triplicate, and average values were reported. Selection of temperatures was made to represent ambient and elevated reservoir-relevant thermal conditions.

3-4 CMC Determination by Conductivity

The CMC of the synthesized Gemini surfactant (T14S3) was determined by electrical conductivity measurements at three temperatures: 25 ± 0.1 °C, 35 ± 0.1 °C, and 45 ± 0.1 °C. Conductivity was measured using a calibrated digital conductivity meter (Model CON 700, Eutech Instruments, Singapore) equipped with a platinum electrode cell (cell constant K = 1.0 cm^{-1}). The instrument was standardized before each measurement series using 0.01 M KCl solution.

Stock solutions of T14S3 were prepared in deionized water and serially diluted to cover a concentration range from below to above the expected CMC. Each solution was equilibrated at the target temperature for 15 min in a thermostated water bath before conductivity readings were recorded. Measurements were made in triplicate, with the electrode rinsed thoroughly between samples to prevent carryover.

Conductivity–concentration data were plotted, and the CMC at each temperature was obtained from the intersection of two linear regression lines corresponding to the pre-micellar and post-micellar regions. The method was applied exclusively to the Gemini surfactant; it was not

used for nanosilica dispersions due to the absence of micellization phenomena in colloidal particulate systems.

3-5 Preparation of Formulated Fluid Systems

A series of aqueous formulations were prepared for interfacial tension, wettability, adsorption, and spontaneous imbibition experiments. The base aqueous phase consisted of either deionized water, sea water or synthetic formation brine (salinity and ionic composition matching the target reservoir). All chemical stock solutions were prepared using Milli-Q water (resistivity > 18.2 MΩ cm) and stored in amber glass bottles at 25 ± 1 °C until use.

For surfactant-containing systems, the synthesized Gemini surfactant T14S3 was dissolved directly in the aqueous phase at the desired concentration, determined either as a fraction or multiple of the critical micelle concentration (CMC) obtained in conductivity measurements. For nanosilica (NS)-containing systems, the required mass of green *Equisetum*-derived NS was gradually added to the aqueous or surfactant solution under continuous magnetic stirring (400 rpm) for 15 min. The dispersion was then ultrasonicated (40 kHz, 120 W) in an ice-bath for 10 min to prevent local heating and ensure uniform particle size distribution.

Electrolyte-modified systems were prepared by dissolving analytical grade sodium sulfate (Na_2SO_4) in the aqueous phase prior to the addition of surfactant or NS. Target salinities were selected based on preliminary optimization studies and ranged from 0 to 10 000 ppm. For ternary systems, Na_2SO_4 was added at the optimum salinity identified from IFT and wettability alteration experiments.

All formulated fluids were allowed to equilibrate for 24 h at the test temperature (25 ± 0.1 °C) to ensure complete dissolution, micellization, and nanoparticle–surfactant interaction prior to testing.

The pH of each formulation was measured (±0.02 units) and, when specified, adjusted to pH 8.0 using a 0.01 M NaOH (to increase pH) or 0.1 M HCl (to decrease pH). Prior to use in experiments, formulations were visually inspected for phase separation or sedimentation, and their conductivity and turbidity were recorded as quality control parameters.

3-6 Interfacial Tension (IFT) Measurement

The interfacial tension between crude oil and aqueous phases containing the synthesized Gemini surfactant (T14S3) was determined using a spinning drop tensiometer (KRÜSS SITE100, Germany) in accordance with ASTM D971-21. All measurements were performed at 25 ± 0.1 °C, with the aqueous phase prepared either in deionized water or containing plant-derived nanosilica (NS) at weight fractions of 0.003, 0.01, and 0.1 wt%. For each test, the surfactant concentration was varied across a range encompassing sub-CMC to post-CMC levels, with solutions equilibrated for 24 h to ensure micellar and particle–surfactant complex stability.

Formulations containing NS were prepared by dispersing the required mass of nanoparticles into the surfactant solution via 15 min magnetic stirring (400 rpm) followed by ultrasonication (40 kHz, 120 W, 10 min) under ice-bath cooling. The crude oil phase was pre-filtered to remove suspended solids and degassed to eliminate air bubbles. In each measurement, the oil droplet volume was adjusted to achieve capillary numbers within the accurate detection range of the instrument; IFT values were recorded after equilibrium (typically within 4–6 min).

To assess electrolyte effects, sodium sulfate (Na_2SO_4) was added at selected concentrations (0–6000 ppm) to formulations containing Gemini surfactant (at ~100ppm) and 0.1 wt% NS. Each Na_2SO_4 stock solution was prepared in deionized water and filtered (0.22 μm) prior to use. IFT values were obtained in triplicate, and the mean values were plotted as a function of surfactant

concentration and electrolyte salinity to determine apparent CMC shifts and optimum salinity conditions.

3-7 Wettability Alteration Test

Wettability alteration of carbonate rock toward oil–water systems in the presence of Gemini surfactant, plant-derived nanosilica, and sodium sulfate was evaluated by contact angle measurements using an optical contact angle goniometer (Model OCA 25, Dataphysics, Germany).

Carbonate rock cores were cut into thin slices (approximately 10 mm × 10 mm × 3 mm), ground to achieve flat surfaces, and polished with 1200-grit SiC paper. To establish an oil-wet condition, the slices were immersed in filtered crude oil (see Section 3-1 for oil properties) and aged at 80 °C for 7 days. Excess oil was gently removed with absorbent paper before initiating measurements.

For the first series of tests, an aqueous phase containing the Gemini surfactant at 1.5×CMC was used as the test fluid. The second series used the same surfactant solution supplemented with 0.1 wt% NS, dispersed via 15 min magnetic stirring at 400 rpm followed by ultrasonication (40 kHz, 120 W, 10 min) in an ice bath. In both cases, the contact angle between the crude oil droplet and the aqueous phase on the rock surface was recorded at time intervals from 0 to 1200 s to evaluate dynamic wettability alteration.

In the third series, the surfactant solution (1.5×CMC), was tested with varying Na_2SO_4 concentrations (0–10000 ppm). Contact angles were measured after 1200 s to determine the optimum salinity for wettability alteration. In the final series, the co-formulated system of surfactant (1.5×CMC) and NS (0.1 wt%) was combined with this optimum Na_2SO_4 concentration, and the resulting contact angles were monitored dynamically to quantify the transition from oil-wet to water-wet conditions.

All measurements were carried out at 25 ± 1 °C, using triplicate rock slices per condition. Contact angles were determined from sessile drop images by fitting the droplet profile with the Young–Laplace equation using the instrument's software.

3-8 Adsorption Measurement

Carbonate outcrop blocks were used for all adsorption experiments. The rock samples were crushed, milled, and sieved to obtain particles in the 75–125 μm range. The sieved powder was washed with acetone, rinsed thoroughly with Milli-Q water (resistivity > 18.2 MΩ cm), and oven-dried at 60 °C for 24 h. To ensure data consistency, all adsorption tests were conducted using the same prepared batch of carbonate powder.

Adsorption measurements were performed by mixing the rock powder with the prepared test solutions at a fixed solid-to-liquid ratio of 1 g rock powder per 100 mL of solution. Stock solutions of the Gemini surfactant T14S3 and green-derived nanosilica were prepared with Milli-Q water, and NS dispersions were sonicated at 100 W for 15 min before dilution. The pH of test solutions was adjusted to 8.00 ± 0.05 using a 0.01 M $NaHCO_3/Na_2CO_3$ buffer where applicable. Single-component isotherms were determined for surfactant solutions (0–300 ppm) in salt-free conditions and in the presence of Na_2SO_4 electrolyte (1000–8000 ppm), as well as for nanosilica dispersions (0–1300 ppm).

From these isotherms, the concentrations corresponding to the plateau region, beyond which no significant increase in adsorption was observed, were chosen for binary and ternary adsorption tests. For the inorganic salt (Na_2SO_4), the concentration that produced the highest adsorption in the single-component tests was selected. Binary systems consisted of surfactant and nanosilica in the buffered medium at pH 8.0, whereas ternary systems additionally contained optimum

concentration of Na_2SO_4. The prepared mixtures were placed in 50 mL glass-stoppered flasks and agitated at 120 rpm for 24 h at 25.0 ± 0.1 °C to reach adsorption equilibrium.

Following equilibration, suspensions were centrifuged at 8000 rpm for 15 min, and the supernatants were filtered through 0.22 µm PTFE syringe filters for analysis. The surfactant concentrations were quantified via UV–Vis spectrophotometry at 220 nm with matrix-matched calibration curves, and selected samples were validated by HPLC using a C18 column. Nanosilica concentrations were determined using the molybdosilicate spectrophotometric method at 410 nm, with inductively coupled plasma optical emission spectrometry (ICP-OES) validation in selected cases.

The equilibrium adsorption capacity (qe) was calculated according to:

$$\boldsymbol{q = \frac{(Co - Ce).V}{m}} \quad (2)$$

where C_0 and Ce are the initial and equilibrium concentrations (mg L^{-1}), V is the solution volume (L), and m is the mass of carbonate powder (g). In multi-component systems, adsorption of each species was compared directly with the corresponding single-component value to determine the Synergy Index, defined as:

$$\boldsymbol{SI = q_{mix} - q_{single}} \quad (3)$$

Finally, adsorption isotherms for all systems were modelled using non-linear regression to the Langmuir and Freundlich equations, with parameters qmax, K_L, K_F, n and R^2 reported for comparative evaluation.

3-9 Spontaneous Imbibition Test

The spontaneous imbibition behavior of carbonate rock was evaluated using an optimized aqueous formulation comprising Gemini surfactant and plant-derived nanosilica at the composition and salinity that yielded the best performance in interfacial tension (IFT) reduction and wettability alteration tests. Core preparation and initial water saturation measurements were conducted using synthetic formation brine formulated to match the ionic composition and salinity of the target reservoir, ensuring realistic reservoir-matched conditions for porosity, permeability, and saturation characterization. For the imbibition tests, two aqueous systems were employed:

(1) a baseline brine prepared using natural seawater (representative of a conventional injection scenario), and

(2) an engineered ternary formulation containing the Gemini surfactant T14S3, green-derived nanosilica, and Na_2SO_4 at concentrations optimized from preceding IFT and contact angle experiments to maximize wettability shift toward water-wetness and minimize interfacial tension, thereby enhancing capillary-driven oil displacement.

Cylindrical carbonate core plugs (length ≈10.0 cm, diameter ≈ 3.81 cm) were oven-dried at 60 °C, vacuum-saturated with synthetic formation brine, and subsequently aged in crude oil at 80 °C for 40 days to re-establish mixed-wet to oil-wet conditions, as verified by the Amott–Harvey index. The detailed physical and petrophysical properties of the cores (porosity, permeability, initial water saturation, and pore volume) are summarized in Table 5.

Table 5. Physical and petrophysical properties of carbonate core plugs

Core	Length (cm)	Diameter (cm)	Porosity (%)	Pore Volume (cm^3)	Initial Water Saturation (S_{wi})
1	10	3.81	15.2	17.32	35
2	10	3.81	15.7	17.9	34
3	10	3.81	15.4	17.55	35

The imbibition tests were conducted using an Amott cell assembly equipped with graduated pipettes to measure oil production volume over time. Each aged oil-saturated core was fully immersed in 100 mL of the prepared aqueous formulation, ensuring complete fluid contact under static conditions. The test temperature was maintained at 85°C using a thermostated water bath to simulate reservoir conditions. The cumulative volume of oil displaced from the core into the calibrated arm of the Amott cell was recorded at defined time intervals (0.5 h, 1 h, 3 h, 6 h, 12 h, 24 h, and daily thereafter) until no further oil production was observed.

3-10 Data Analysis and Oil Recovery Calculation

Oil recovery during spontaneous imbibition was calculated using the volumetric method, based on cumulative oil production data obtained from the Amott cell measurements. For each core sample, the volume of displaced oil collected in the graduated arm of the Amott cell was recorded at defined time intervals and expressed at ambient conditions. Measured volumes were corrected for any potential contraction or expansion due to the temperature difference between reservoir test temperature and laboratory reference conditions.

The original oil in place (OOIP) for each core plug was determined from the measured pore volume (PV) and irreducible water saturation (Swi), according to:

$$\boldsymbol{OOIP = PV \times (1 - S_{wi})} \quad (4)$$

The imbibition oil recovery factor (RF_{SI}) at any time t was calculated as:

$$\boldsymbol{RF_{SI}(t) = \frac{V_{o,cum}(t)}{OOIP} \times 100} \quad (5)$$

where $V_{o,cum}(t)$ is the cumulative volume of oil produced (cm^3) at time t.

4- Result and Discussion

4-1 Overview of Findings

This study integrated a temperature-responsive, plant-derived nanosilica, a novel cationic Gemini surfactant (T14S3), and tailored salinity adjustment via Na_2SO_4 to enhance oil recovery in carbonate systems through synergistic interfacial engineering. Comprehensive material characterization confirmed the distinct structural and surface properties underpinning their cooperative performance: the carbonate rock exhibited a well-ordered calcite lattice with sharp XRD reflections, whereas the Equisetum-derived nanosilica displayed an amorphous high-surface-area silicate network, offering abundant silanol groups and residual organics conducive to surfactant–particle interactions. FTIR and ^{1}H-NMR analyses verified the successful synthesis of T14S3 with its bis-quaternary headgroups and long hydrophobic tails, while TGA profiles demonstrated sufficient thermal stability of both surfactant and nanoparticle phases for EOR applications.

Electrokinetic and colloidal studies revealed that nanosilica imparted strong negative surface charges across the pH spectrum, promoting water wetness, whereas T14S3 maintained a positive charge over broad pH ranges, favoring robust adsorption on carbonate. Na_2SO_4 addition enabled precise tuning of these interfacial charges via divalent anion adsorption and double-layer

compression, directly influencing particle stability and adsorption capacities. Interfacial tension (IFT) and wettability alteration tests revealed distinct optima: the lowest IFT (~0.51 mN/m) occurred at higher salinity (5 500 ppm Na_2SO_4), whereas the most pronounced wettability shift (final contact angle ~34°) was achieved at moderate salinity (2 000 ppm Na_2SO_4). Adsorption modeling indicated Langmuir-type monolayer coverage for both components, with binary and ternary systems exhibiting positive synergies. Spontaneous imbibition results corroborated these findings, showing that the optimized ternary formulation nearly doubled oil recovery compared to baseline brine, with wettability shift emerging as the dominant recovery mechanism and IFT reduction playing a secondary, yet complementary, role.

4-2 Characterization Results of Materials

4-2-1 XRD Results

The X-ray diffraction (XRD) pattern of the carbonate reservoir core sample (Figure 2) exhibited multiple sharp and intense peaks across the 2θ range, with the most prominent reflection observed at approximately 39.4° (2θ) with an intensity exceeding 13,000 A.U. Additional strong reflections appeared at ~23.1°, 29.5°, 43.1°, 47.5°, and 48.6°. The presence of these sharp, well-defined peaks indicates a high degree of crystallinity, characteristic of calcite ($CaCO_3$) as the dominant mineral phase. These results are in agreement with standard JCPDS data for crystalline calcite structures, confirming the mineralogical purity and well-ordered lattice of the rock material.

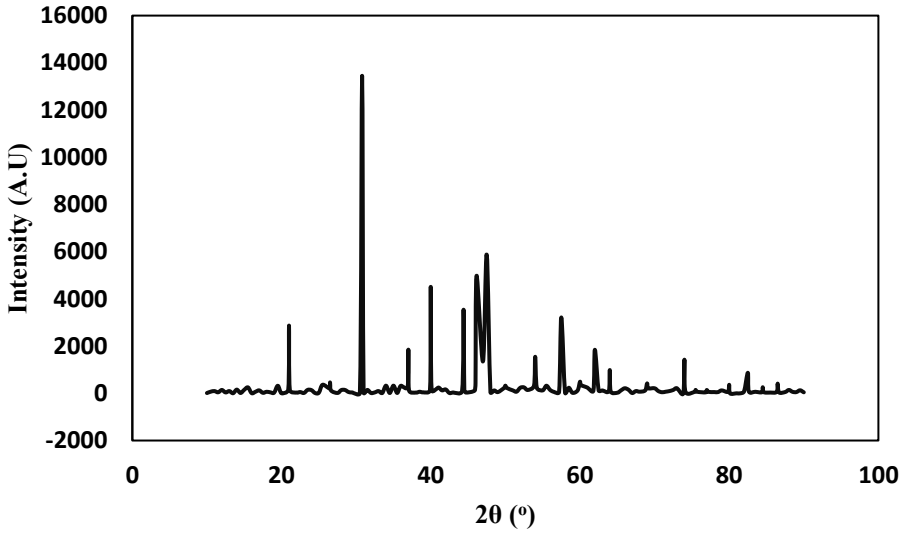

Figure 2. *X-ray diffraction (XRD) pattern of the carbonate reservoir rock sample*

In contrast, the XRD profile of the plant-derived nanosilica (Figure 3) presented a single broad diffraction hump centered around 25° (2θ) with a relatively low intensity (~410 A.U), and no sharp crystalline peaks were detected. This diffuse halo is a typical signature of amorphous silica, reflecting the absence of long-range periodic atomic arrangements and the presence of a highly disordered silicate network.

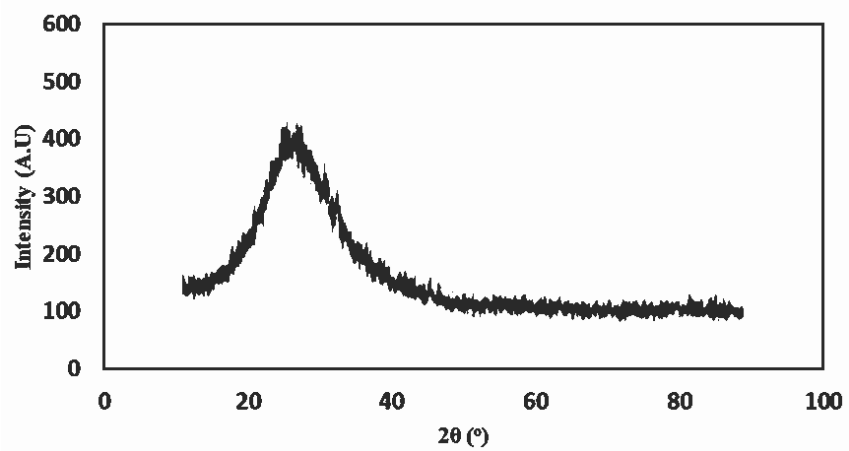

Figure 3. *X-ray diffraction (XRD) pattern of the Equisetum arvense derived nanosilica*

The amorphous nature likely arises from the biogenic origin of the material and the preparation route, which typically avoids high-temperature crystallization steps. This structural disorder contributes to the large specific surface area and abundant surface silanol groups, beneficial for chemical functionalization and synergistic interactions with the Gemini surfactant in EOR applications.

4-2-2 FTIR Results

The FTIR spectrum of the synthesized Gemini surfactant (T14S3) (Figure 4) displayed characteristic absorption bands confirming its molecular structure. The strong peaks at approximately 2921 and 2852 cm^{-1} correspond to the asymmetric and symmetric stretching vibrations of $–CH_3$/$–CH_2$ alkyl chains, which are typical for long hydrophobic tails. A distinct absorption at ~1470 cm^{-1} is assigned to $–CH_3$ bending modes, whereas the medium-intensity bands at ~1245 and 1170 cm^{-1} are associated with C–N stretching vibrations. A sharp and intense band near 960–970 cm^{-1} corresponds to the stretching of the quaternary ammonium group (R_4N^+), validating the cationic headgroup incorporation. The small peak observed in the region 720–730 cm^{-1} is attributed to rocking vibrations of the $(CH_2)_n$ segment, confirming long alkyl chain packing. These functional group assignments are in full agreement with the expected gemini quaternary ammonium surfactant structure.

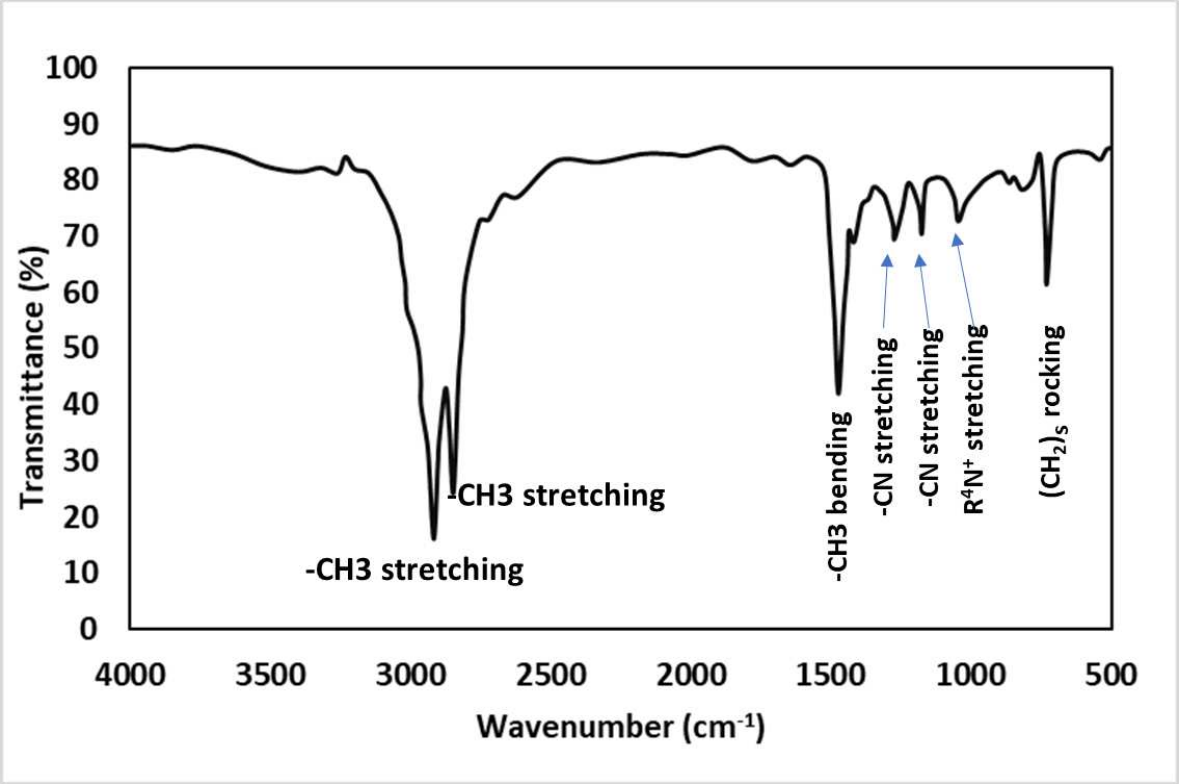

Figure 4. The FTIR spectrum of the synthesized Gemini surfactant (T14S3)

The comparative FTIR spectra of commercial pure silica and plant-derived nanosilica from *Equisetum arvense* (Figure 5) revealed the typical vibrational features of amorphous SiO_2 and additional signals arising from the biogenic origin of the material. Both spectra exhibit a prominent broad peak centered at 1060–1080 cm^{-1}, assigned to Si–O–Si asymmetric stretching, along with a shoulder around ~800 cm^{-1} (symmetric Si–O stretching) and a band near 460–470 cm^{-1} (O–Si–O bending). In the *Equisetum*-derived silica, a broad OH stretching band appeared at ~3400 cm^{-1} and an H–O–H bending mode at ~1630 cm^{-1}, indicating the presence of surface hydroxyls and adsorbed molecular water. Additionally, weak absorptions near 2920 and 2850 cm^{-1} correspond to residual $–CH_2$/$–CH_3$ groups, while the bands around 1730 cm^{-1} (C=O), 1510 cm^{-1} (aromatic C=C), and ~1250 cm^{-1} (C–O) suggest trace lignocellulosic residues from the plant matrix. These organic residues may enhance interfacial activity and create synergistic interactions with the Gemini surfactant in oil recovery applications.

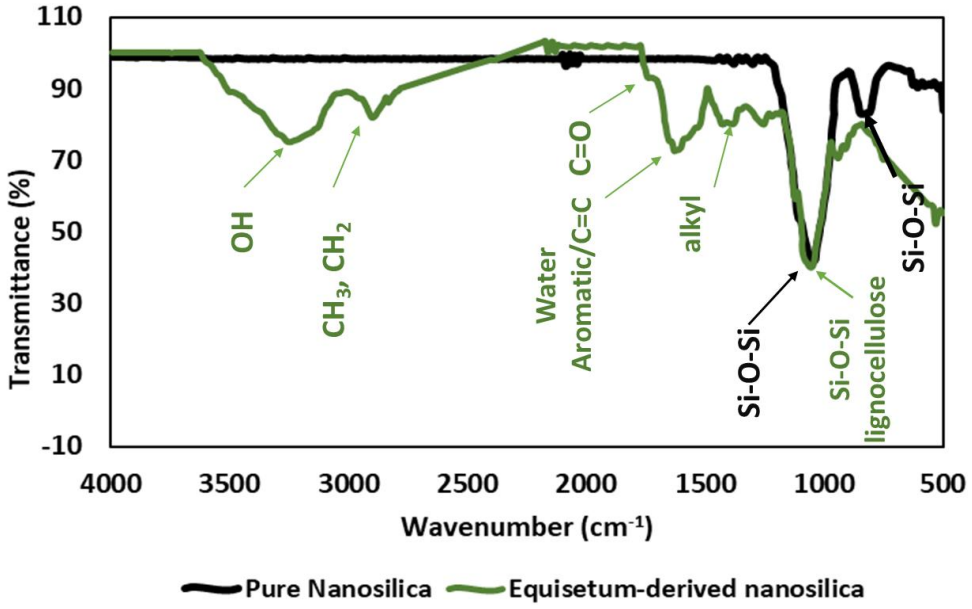

Figure 5. The FTIR spectrum of commercial pure silica and plant-derived nanosilica from Equisetum arvense

Overall, the FTIR results validate the successful synthesis of the Gemini surfactant (T14S3) with its expected cationic–hydrophobic duality, and confirm the amorphous silicate framework of the plant-derived nanosilica while preserving surface hydroxyls and minor organic moieties. The combination of these two materials offers complementary functionalities: hydrophilic–reactive silanol surfaces from the silica and amphiphilic–cationic activity from the gemini surfactant, potentially enhancing wettability alteration and interfacial tension reduction in carbonate reservoir conditions.

4-2-3 ^{1}H-NMR Results

The ^{1}H-NMR spectrum of the synthesized Gemini surfactant provides unequivocal evidence of its molecular architecture through well-resolved proton resonance assignments. The multiplet at δ 3.692–3.709 ppm corresponds to α-methylene protons adjacent to the quaternary ammonium centers, while the spacer methylene groups directly bound to the N^{+} headgroups appear at δ 3.298–3.384 ppm. A distinct singlet at δ 3.03–3.11 ppm is assigned to the $N^{+}(CH_3)_2$ methyl protons,

collectively confirming the characteristic bis-quaternary headgroups and symmetric spacer chain of the Gemini structure, as illustrated in Figure 6.

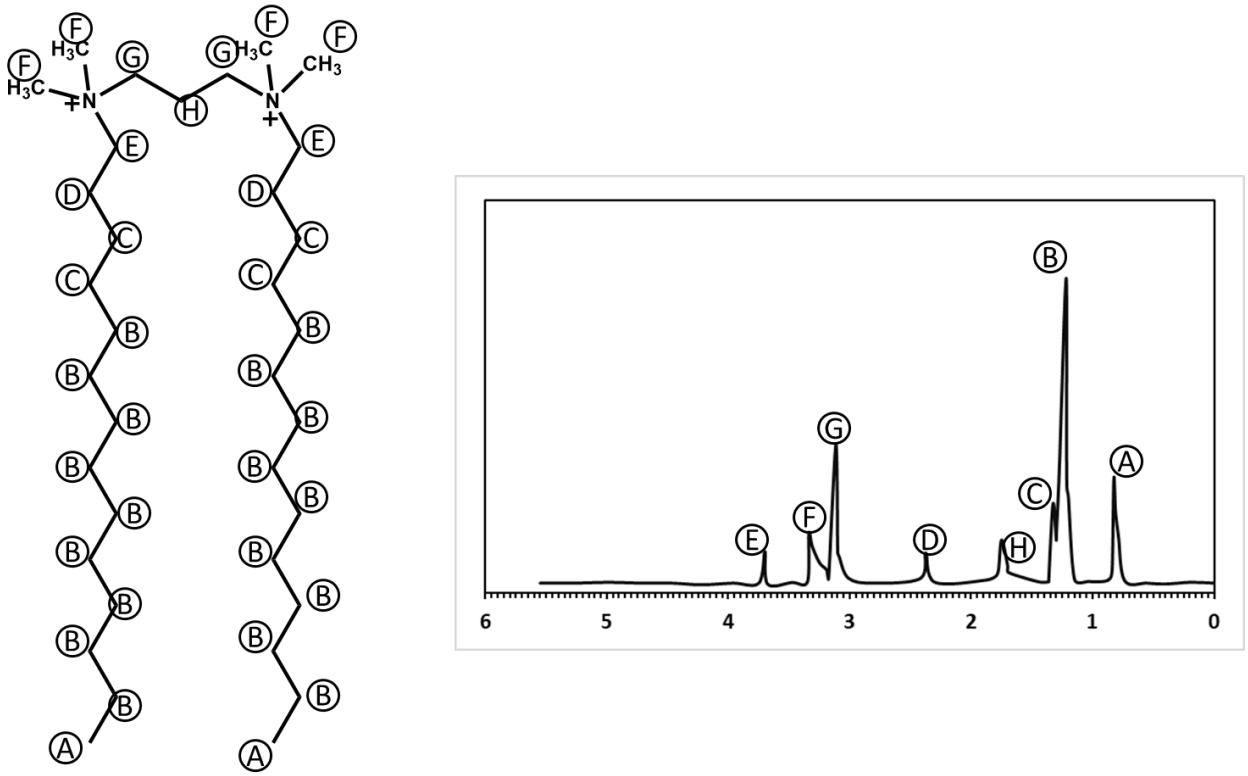

Figure 6. 1H-NMR spectrum of the synthesized Gemini surfactant (T14S3).

The β-methylene protons within the hydrophobic tail exhibit a characteristic resonance at δ 2.367–2.372 ppm, whereas the central methylene group in the polymethylene spacer resonates at δ 1.711–1.719 ppm. The γ-methylene protons are observed at δ 1.323–1.329 ppm, followed by an intense signal at δ 1.218–1.224 ppm arising from the long-chain methylene segment (C5–C13). Finally, the terminal methyl groups (C14) appear in the upfield region at δ 0.796–0.826 ppm. These resonance assignments, together with the previously discussed quaternary ammonium headgroup signals, are comprehensively summarized in Table 6.

Table 6. ^{1}H-NMR chemical shift assignments and proton integration values for the synthesized Gemini surfactant, corresponding to structural positions.

Assignment	Position in Chemical Structure (Figure 6)	δ (ppm)	Relative integral (H)
C1 α-methylene protons adjacent to quaternary ammonium center	E	3.692-3.709	2
Spacer $–CH_2–$ units adjacent to N^+ headgroups	G	3.298–3.384	2
$N^+(CH_3)_2$ methyl protons	F	3.03-3.11	6
β-methylene protons in hydrophobic tail	D	2.367-2.372	2
Central CH_2 in polymethylene spacer	H	1.711-1.719	1
γ-methylene protons in hydrophobic tail	C	1.323-1.329	4
Long-chain methylene protons (C5–C13)	B	1.218-1.224	18
Terminal methyl protons (C14)	A	0.796–0.826	3

The sharpness and integration ratios of these peaks are consistent with the expected structure of the synthesized cationic Gemini surfactant, verifying the successful quaternization and incorporation of long hydrophobic alkyl chains.

4-2-4 TGA Results

The thermal stability and compositional characteristics of the synthesized Gemini surfactant and nanosilica samples were evaluated by thermogravimetric analysis (TGA) (Figure 7(a–b)).

For the Gemini surfactant (Figure 7.a), the TGA curve recorded from 30 °C to 300 °C reveals three distinct regions. The initial weight loss of approximately 2–3% below 120 °C is attributed to the evaporation of physically adsorbed moisture. A major weight loss of about 40–45% occurs between 200 °C and 270 °C, corresponding to the thermal degradation of the organic backbone and quaternary ammonium headgroups. Beyond this temperature, the remaining mass approaches ~55%, indicating the presence of residual char and thermally stable fragments.

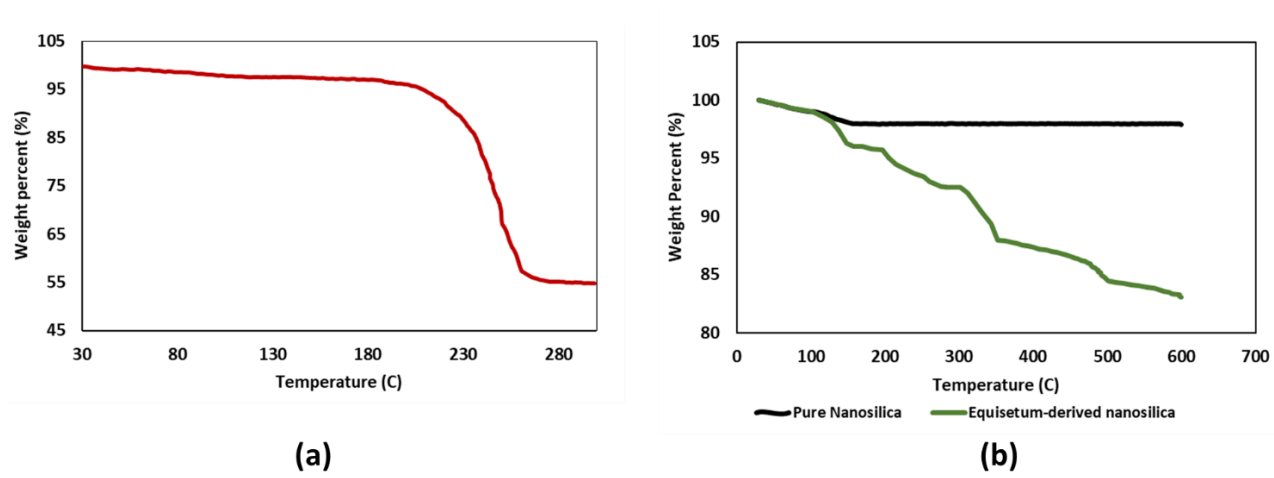

Figure 7. TGA profiles of (a) Synthesized Gemini Surfactant and (b) pure nanosilica and Equisetum-derived nanosilica

In contrast, the TGA profiles of pure nanosilica and *Equisetum*-derived nanosilica (Figure 7.b) were recorded up to 600 °C due to their significantly higher inorganic content. The commercial nanosilica shows minimal weight loss (~2–3%) over the entire temperature range, confirming its high purity and thermal stability. The TGA curve of the plant-derived nanosilica shows an initial weight loss of about 3–4% below 150 °C, which is attributed to the removal of physically adsorbed water. This is followed by a gradual 5–7% decrease in mass between 150 °C and 350 °C, corresponding to the thermal decomposition of residual organic matter originating from the *Equisetum* precursor. At higher temperatures, from 350 °C to 600 °C, a further 3–5% weight loss is observed, which is related to the oxidation of carbonaceous residues and traces of organics trapped within the silica network. The extended temperature range for silica samples was selected to ensure complete removal of these residual organic components and to clearly distinguish their thermal stability from that of commercial nanosilica.

4-2-5 Zeta Potential Results

The zeta potential–pH behavior of the bare carbonate rock powder, the individual phases, and their mixtures is shown in Figure 8. For the unmodified rock, the curve started at approximately +22 mV

at pH 4.0, consistent with dominant protonated surface carbonate species ($CaOH_2^+$) in acidic media. The potential decreased progressively with increasing pH, crossing zero near pH 8.4 and becoming negative above this point as surface deprotonation of CaOH groups into CaO^- occurred. In literature, the point of zero charge (PZC) for calcite spans a wide range (5.4–10.8) depending on mineral origin, salt content, and measurement conditions {Bazyari, 2025 #658}. Some studies report positively charged calcite in deionized water, while others observe a negative charge. These discrepancies arise from the complex dissolution equilibria of calcite in aqueous systems, where concurrent release of Ca^{2+}, HCO_3^-, and CO_3^{2-} ions make an intuitive prediction of surface charge difficult. The dissolution reactions ($CaCO_3 \rightleftharpoons Ca^{2+} + CO_3^{2-}$; $CO_3^{2-} + H_2O \rightleftharpoons HCO_3^- + OH^-$; $HCO_3^- + H_2O \rightleftharpoons H_2CO_3 + OH^-$; …) generate both cations and anions in solution. Because the energy barrier for releasing Ca^{2+} from the lattice is lower than that for CO_3^{2-}, calcium vacancies form more readily, imparting a net negative charge to the surface. This mechanistic explanation is consistent with our observation.

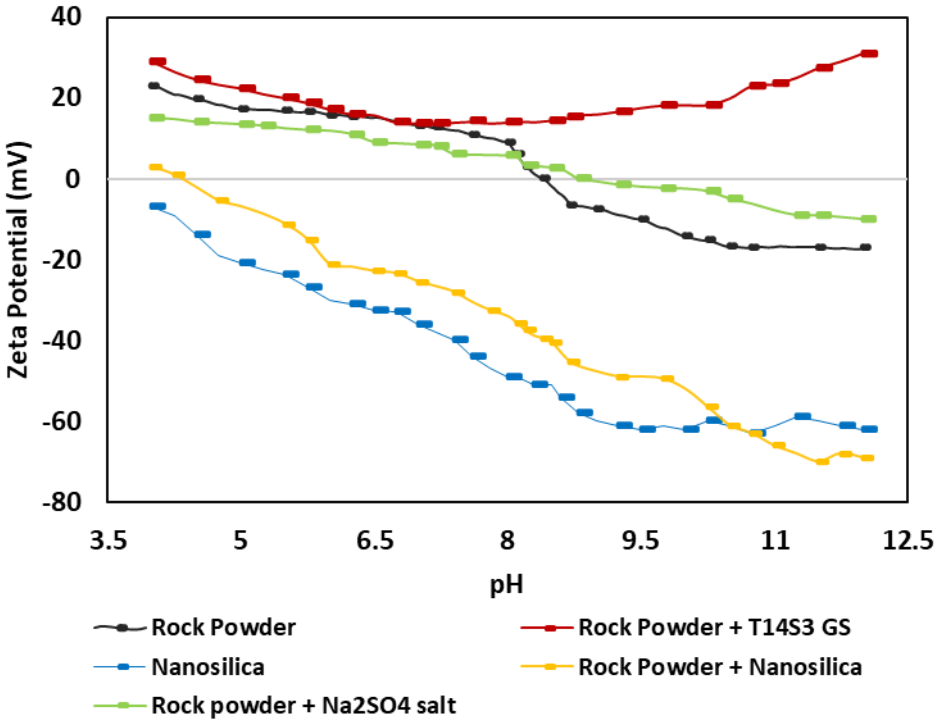

Figure 8. Zeta potential of carbonate rock and its modifications with nanosilica, Na_2SO_4, and Gemini surfactant T14S3 across pH range.

The introduction of Na_2SO_4 shifted the entire curve toward less negative or less positive values and displaced the PZC to ~pH 8.8. This reflects specific adsorption of sulfate anions onto positively charged surface sites at acidic–neutral pH, coupled with electrical double-layer compression due to increased ionic strength. Both effects diminish the magnitude of the zeta potential while stabilizing deprotonated states at higher pH.

The nanosilica phase alone displayed strongly negative potentials over the entire pH range, from −10 mV at pH 4.0 to ≤ −65 mV above pH 10, due to deprotonation of abundant surface silanol groups (Si–OH → Si–O^-). This high charge density enhances electrostatic stabilization in alkaline environments.

When combined with rock powder, nanosilica rendered the composite system more negative than the bare rock, especially at high pH, reflecting partial surface coverage of carbonate particles by

nanosilica and the transfer of silica's electrokinetic signature to the composite surface. Such heteroaggregation masks part of the carbonate surface, reducing the influence of its PZC and shifting the net potential toward nanosilica's strongly negative values.

By contrast, adsorption of the Gemini surfactant T14S3 preserved a high positive surface charge from acidic to strongly alkaline conditions. The cationic headgroups anchor strongly to carbonate sites through electrostatic attraction, while hydrophobic interactions between the alkyl tails promote dense monolayer formation. This coating effectively suppresses deprotonation of carbonate groups, preventing negative charge development even in high-pH environments.

Mechanistically, the data illustrate the combined influence of (i) surface acid–base equilibria tied to mineral group speciation, (ii) specific ion adsorption altering double-layer structure and net charge, and (iii) surface modification through nanoparticles or surfactants that change both the magnitude and sign of the zeta potential. These processes have direct implications for enhanced oil recovery (EOR): positively charged surfaces tend to stabilize oil films through electrostatic attraction, whereas highly negative surfaces encourage water wetting and oil displacement efficiency. The tunability demonstrated here, ranging from strongly negative (nanosilica) to strongly positive (T14S3), offers strategic flexibility for wettability alteration in carbonate reservoirs.

4-2-6 DLS Results

The particle size distributions of the green-synthesized plant-derived nanosilica and the Gemini surfactant T14S3 are presented in Figure 9 (a, b). Figure 9.a shows the nanosilica dispersion at a concentration of 0.02 wt%, with a single dominant peak centered at approximately **70 nm**. This indicates that most particles fall within the optimal range for reservoir penetration while

maintaining sufficient surface area for adsorption and wettability modification. The moderate distribution width suggests slight polydispersity, likely due to weak secondary aggregation from van der Waals interactions during suspension preparation. The absence of large particles (> 1 μm) minimizes the risk of pore plugging in carbonate formations.

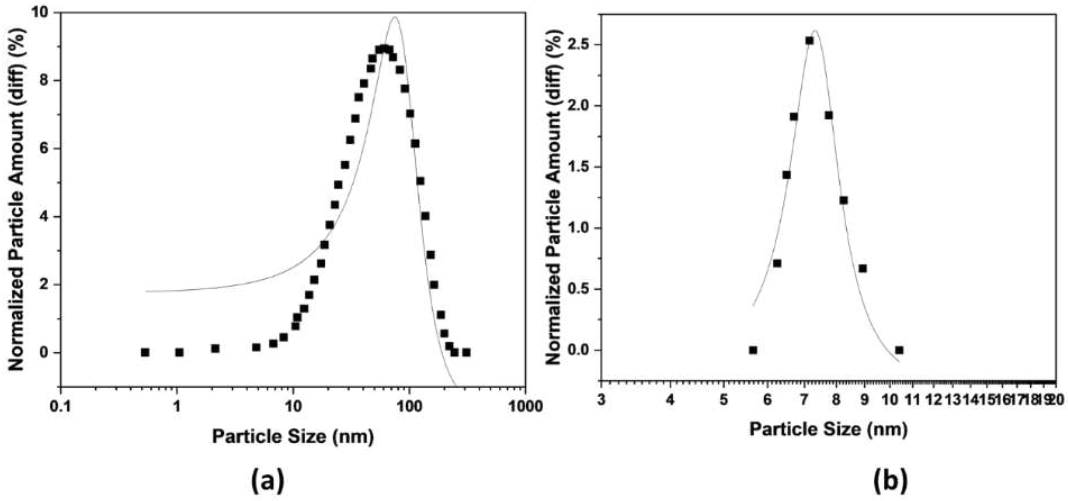

Figure 9. Particle size distribution of green-synthesized plant-derived nanosilica (a) and Gemini surfactant aggregates (b), with faint lines indicating Gaussian distribution fits.

Figure 9.b depicts the distribution profile of Gemini surfactant T14S3 at 80 ppm (~CMC), revealing a narrow monomodal peak at approximately 7.5 nm, corresponding to the hydrodynamic diameter of micellar aggregates in aqueous media. The tight distribution indicates uniform aggregate formation, which favors stable transport through porous media and effective interfacial tension reduction in EOR applications.

Curve fitting with Gaussian and Lorentzian models was used to further quantify the distribution sharpness and symmetry of particle sizes for both nanosilica and Gemini surfactants.

As shown in Table 7, the Gaussian model yielded a higher coefficient of determination ($R^2 = 0.889$) for plant-derived nanosilica compared to the Lorentzian model ($R^2 = 0.8479$), indicating a distribution closer to a normal profile with moderate tailing.

In contrast, Gemini surfactants exhibited similarly high R^2 values for both Gaussian (0.9471) and Lorentzian (0.9437) fits, reflecting the distribution's narrow width and symmetrical shape.

Table 7. R^2 values for Gaussian and Lorentzian models applied to DLS particle size distributions.

Sample	Gaussian Distribution R^2	Lorentzian Distribution R^2
plant-derived Nanosilica	0.889	0.8479
Gemini Surfactants	0.9471	0.9437

The distinction in particle size between nanosilica and Gemini surfactants implies complementary functional roles in EOR: the larger nanosilica particles can provide mobility control and alter wettability, while the smaller Gemini aggregates facilitate effective IFT reduction and access to finer pores, potentially yielding synergistic enhancements in oil recovery efficiency.

4-2-7 Colloidal Stability Results of Plant-Derived Nanosilica

Table 8 summarizes the stability performance of green-derived nanosilica dispersions in various brine chemistries and temperatures, assessed through Sedimentation Index (SI) and Turbidity Retention after 30 days.

Table 8. Stability data of Equisetum-derived NS dispersions (0.1 wt%) over 30 days

Formulation Code	Medium Composition	Temp (°C)	SI at Day 30 (%)	Turbidity Retention (%)
NS-DIW	Deionized Water	25	2	97
NS-DIW	Deionized Water	60	4	94
NS-2000Na_2SO_4	2000 ppm Na_2SO_4	25	3	96
NS-2000Na_2SO_4	2000 ppm Na_2SO_4	60	5	92
NS-5500Na_2SO_4	5500 ppm Na_2SO_4	25	15	84
NS-5500Na_2SO_4	5500 ppm Na_2SO_4	60	22	78
NS-10000Na_2SO_4	10000 ppm Na_2SO_4	25	28	69
NS-10000Na_2SO_4	10000 ppm Na_2SO_4	60	35	60

NS+GS-5500Na_2SO_4	Gemini T14S3 + 5500 ppm Na_2SO_4	25	10	88
NS+GS-5500Na_2SO_4	Gemini T14S3 + 5500 ppm Na_2SO_4	60	14	82

Mechanistic Trends and Interpretation

- *Low-salinity media (DIW, 2000 ppm Na_2SO_4);* Dispersions retained over 92–97% turbidity with minimal sedimentation (< 5%). Stability arises from strong electrostatic repulsion between highly negative silica surfaces, supported by an extended electrical double layer in low-ionic strength conditions.
- *Moderate salinity (5500 ppm Na_2SO_4);* Noticeable decline in stability (SI rises to 15–22%) due to sulfate-induced double-layer compression, which reduces the Debye length and promotes van der Waals-driven aggregation. The drop is more severe at 60 °C, where increased Brownian motion accelerates particle collisions.
- *High salinity (10 000 ppm Na_2SO_4);* Severe aggregation and sedimentation occur (SI up to 35%, turbidity retention as low as 60%). Here, charge screening is nearly complete, and silica particles interact primarily through London dispersion forces, leading to networked floc formation.
- *Effect of Gemini surfactant (NS+GS in 5500 ppm Na_2SO_4);* Incorporation of cationic T14S3 markedly improves stability compared to NS-5500Na_2SO_4 alone (SI reduced by ~33%, turbidity retention increased by ~8%). This enhanced stability likely results from electrosteric stabilization: positively charged headgroups adsorb to NS surfaces while

hydrophobic tails and hydrated counterions generate a steric barrier, reducing close approach between particles.

Overall, these findings confirm that green-derived nanosilica dispersions are intrinsically stable in low-salinity environments but require surface modification (e.g., Gemini surfactant) to maintain colloidal integrity under moderate-to-high salinity and elevated temperature, conditions that are common in carbonate reservoir EOR operations.

4-3 Conductivity Study and CMC determination

The variation of specific conductivity with Gemini surfactant T14S3 concentration at three different temperatures (25 °C, 35 °C, and 45 °C) is illustrated in Figure 10. In all cases, conductivity increased almost linearly with concentration up to a distinct breakpoint, beyond which the slope decreased, indicating the onset of micellization. This behavior is characteristic of ionic surfactants, where increased ion binding and reduced free ion mobility occur after micelle formation. The observed breakpoints, corresponding to the critical micelle concentration, decreased systematically with increasing temperature, reflecting the enhanced hydrophobic interactions between surfactant tails at elevated thermal energy.

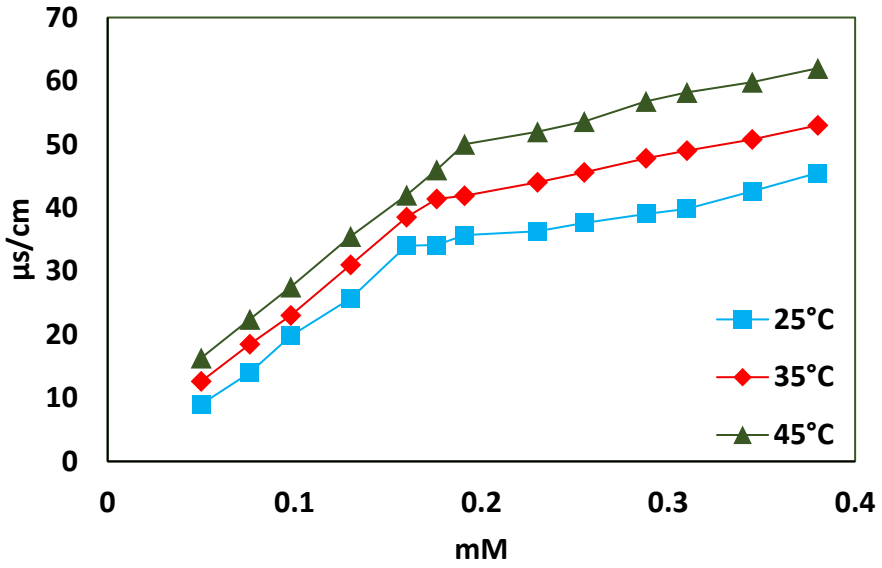

Figure 10. CMC determination of Gemini surfactant T14S3 at 25 °C, 35 °C, and 45 °C from conductivity–concentration plots.

Based on the molecular weight of 525 g mol^{-1}, the experimentally determined CMC values were calculated as 84 ppm at 25 °C, 92.4 ppm at 35 °C, and 100.3 ppm at 45 °C. This decreasing trend confirms that micellization is thermodynamically favored at higher temperatures, likely due to both entropy gain from structured water release and reduced hydration of the head groups. Such temperature dependence is advantageous for EOR applications in reservoirs with moderate to high formation temperatures, as lower CMC values translate to lower surfactant dosages needed to achieve optimal performance in wettability alteration and interfacial tension reduction.

4-4 Interfacial Tension Analysis

The interfacial tension (IFT) behaviour of the Gemini surfactant T14S3 was first investigated in deionized water (DW) and in the presence of nanosilica (NS) at three loadings: 0.003, 0.01, and 0.1 wt% (Figure 11). In the absence of nanoparticles, increasing surfactant concentration reduced the IFT between crude oil and aqueous phase from ~34 mN/m to ~0.91 mN/m, with a distinct breakpoint at ~80 ppm, corresponding to the critical micelle concentration (CMC). Upon adding nanosilica, the IFT–concentration curves shifted slightly towards lower concentrations, and the

minimum IFT was further reduced. At the highest nanoparticle loading (0.1 wt%), the IFT reached ~0.62 mN/m, confirming a strong synergistic effect between the nanoparticle and surfactant.

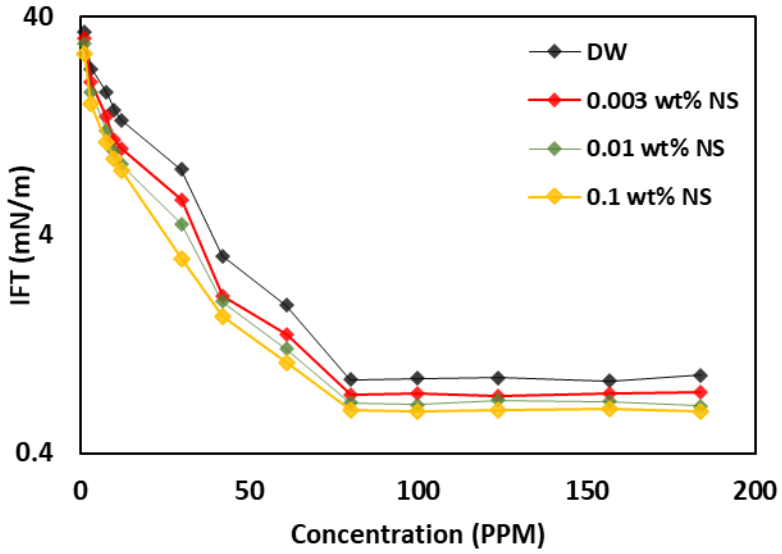

Figure 11. IFT reduction of Gemini surfactant T14S3 with and without nanosilica (0.003–0.1 wt%).

This enhancement is attributed to multiple cooperative mechanisms; 1) Electrostatic attraction between the cationic headgroups of T14S3 and the negatively charged nanosilica surfaces concentrates active molecules near the oil–water interface. 2) Formation of hybrid interfacial films where surfactant–particle complexes pack densely, lowering the interfacial free energy. 3) Nanosilica-induced micelle nucleation by creating localised surfactant-rich regions ("hotspots") that accelerate interfacial saturation.

Based on these findings, sodium sulfate (Na_2SO_4) was selected as a co-additive for salinity optimization due to the strong divalent charge-screening ability of SO_4^{2-} ions, its natural compatibility with carbonate brines, and its capacity to compress the electrical double layer without inducing premature nanoparticle aggregation.

Subsequent tests fixed the surfactant concentration above its measured CMC (~100 ppm) and maintained 0.1 wt% nanosilica, varying Na_2SO_4 concentrations from 0 to 10000 ppm (Figure 12).

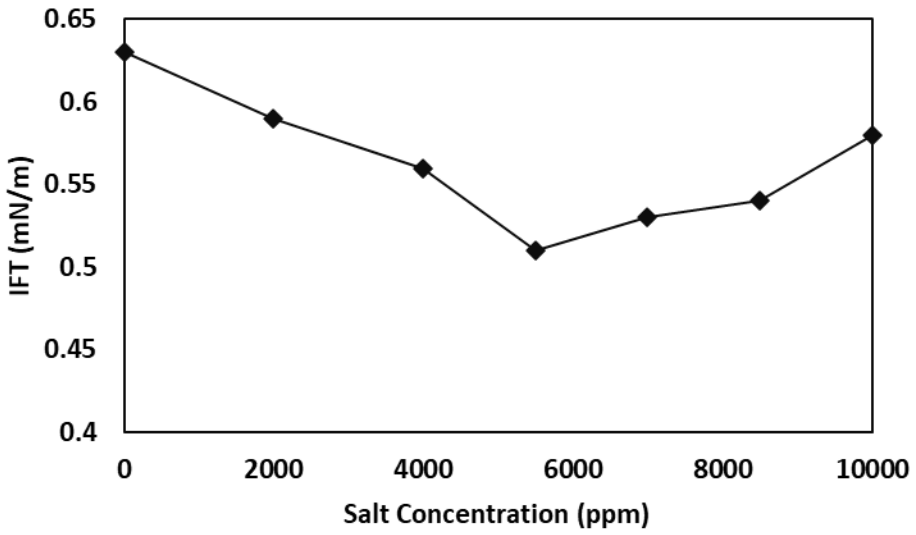

Figure 12. IFT of T14S3 + 0.1 wt% nanosilica at CMCs in various Na_2SO_4 concentration;

The IFT steadily decreased with increasing salt dosage, achieving a minimum value of ~0.51 mN/m at 5500 ppm Na_2SO_4. This behaviour is explained by reduced electrostatic repulsion between surfactant headgroups, increased interfacial packing density, and enhanced nanoparticle adsorption due to double-layer compression. At the optimum salinity, the synergy between T14S3, nanosilica, and sulfate ions produces a stable, compact, and highly efficient interfacial structure in the ultralow IFT regime (< 1 mN/m), which is highly beneficial for mobilising residual oil in carbonate reservoirs.

Beyond the optimum concentration, excessive screening promotes bulk micelle formation and nanoparticle aggregation in the aqueous phase, depleting active species from the interface and slightly increasing IFT values. Overall, these results demonstrate that combining a cationic Gemini surfactant, green-derived nanosilica, and optimised Na_2SO_4 salinity can significantly lower IFT through complementary electrostatic, steric, and colloidal stabilisation mechanisms.

4-5 Wettability Alteration Analysis

Dynamic contact angle measurements (Figure 13) revealed a progressive shift in carbonate rock wettability from an initial oil-wet state toward increased water-wetness for all tested formulations. In the baseline case, the Gemini surfactant solution (1.5×CMC) reduced the initial contact angle from ~138° to ~59° after 1200 s. This change is primarily attributed to the adsorption of cationic Gemini headgroups onto the negatively charged carbonate surface, leading to the displacement of crude oil polar components (asphaltenes, resins) and the formation of a hydrated surfactant layer that facilitates water spreading.

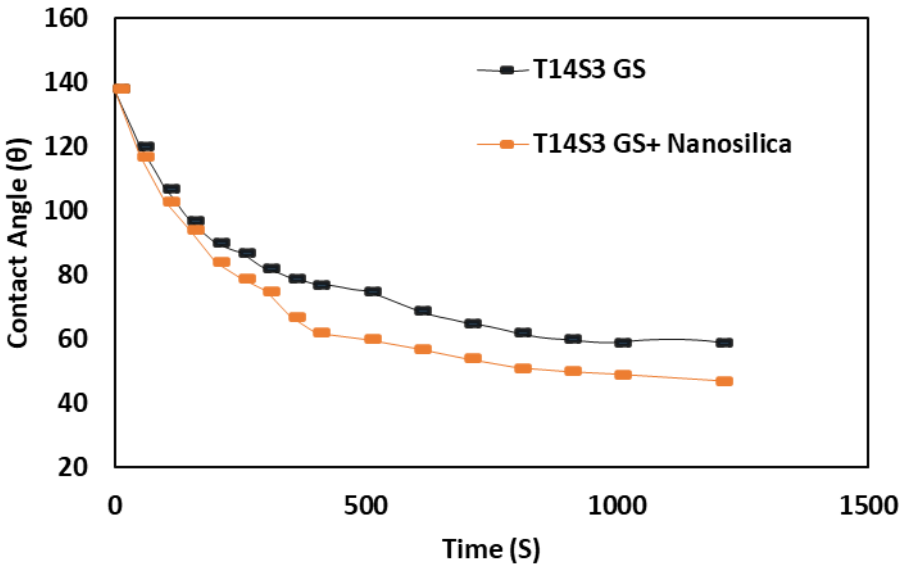

Figure 13. Dynamic contact angle variation for Gemini surfactant alone, and with nanosilica (0.1 wt%).

When 0.1 wt% plant-derived nanosilica was incorporated, the final contact angle decreased further to ~47°. The high surface area and strongly negative charge of nanosilica promote electrostatic bridging with the cationic surfactant, yielding stable hybrid interfacial structures. These structures increase disjoining pressure at the oil–rock–water interface, assisting in oil film rupture and reducing three-phase contact line pinning, thereby accelerating the wettability transition rate observed in Figure 13.

The optimisation of aqueous salinity, performed using Na_2SO_4 (Figure 14), indicated an optimum at 2000 ppm, reducing the static contact angle to ~44° after 1 200 s. This behaviour can be explained by specific adsorption of SO_4^{2-} ions on calcite, combined with electrical double-layer compression, which promotes denser surfactant packing without inducing aggregation. At higher salt concentrations, partial reversal of the contact angle trend was observed, consistent with bulk micelle formation and reduced interfacial availability of active species.

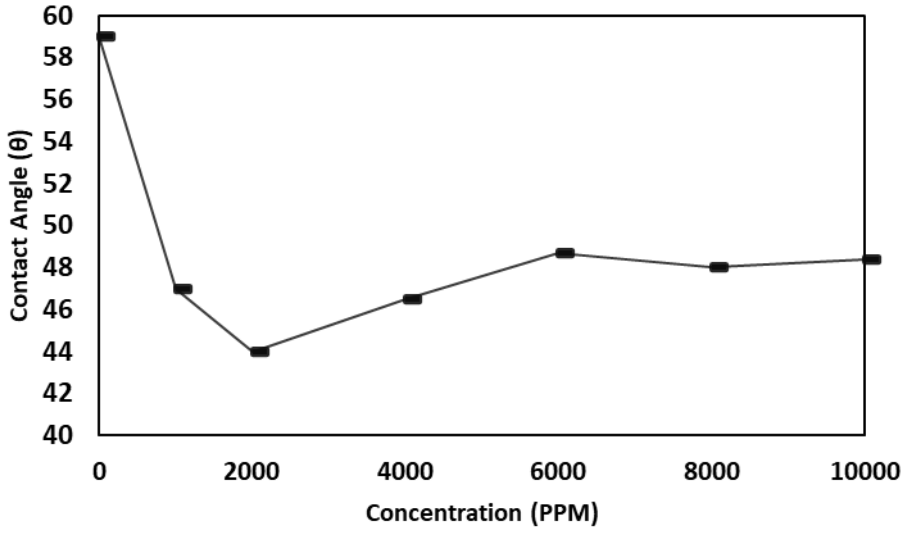

Figure 14. Final contact angle after 1200 s for Gemini surfactant (1.5×CMC) at different Na_2SO_4 concentrations

The most pronounced wettability alteration occurred with the ternary formulation of Gemini (1.5×CMC), nanosilica (0.1 wt%), and Na_2SO_4 (2 000 ppm), where the final contact angle reached ~34° after 1200 s (Figure 15). This superior performance reflects the synergy of three concurrent mechanisms: (i) Electrostatic tuning – optimal charge screening enhances surfactant and nanoparticle adsorption; (ii) Interfacial film reinforcement – hybrid surfactant–nanoparticle layers form dense, hydrophilic coatings; (iii) Capillarity modification, combined IFT reduction and rock surface energy alteration lower the capillary forces resisting oil displacement.

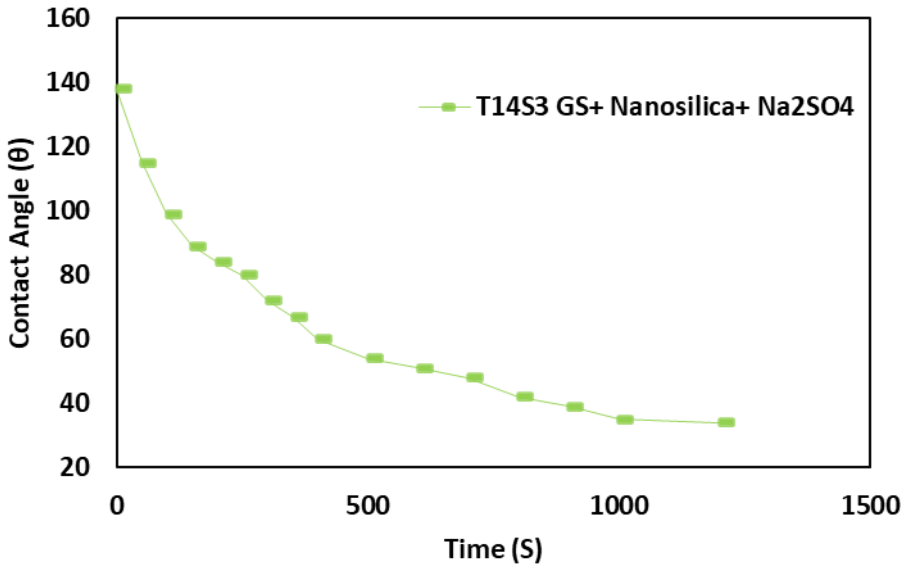

Figure 15. Dynamic contact angle variation for the ternary system: Gemini (1.5×CMC), nanosilica (0.1 wt%), and Na_2SO_4 (2 000 ppm).

Collectively, these results confirm that integrating surface-active molecules, hydrophilic nanoparticles, and tailored ionic strength is a potent strategy for achieving rapid and sustainable wettability reversal in carbonate reservoirs.

4-6 Adsorption Analysis and Modeling

Single-component adsorption isotherms demonstrated distinct uptake behaviors for the Gemini surfactant T14S3 and the green-derived nanosilica on carbonate surfaces (Figures 16 and 17). In deionised water, Gemini uptake rapidly increased at low equilibrium concentrations ($C_e < 100$ ppm), reaching a plateau of ~0.71 mg g^{-1} rock at 300 ppm. The presence of Na_2SO_4 (1000–8000 ppm) systematically enhanced adsorption, with the highest capacity (~0.83 mg g^{-1}) achieved at 2200 ppm. This enhancement is attributed to electrical double layer (EDL) compression and specific adsorption of SO_4^{2-} anions, which reduce electrostatic repulsion between cationic Gemini headgroups, enabling denser packing at the rock interface.

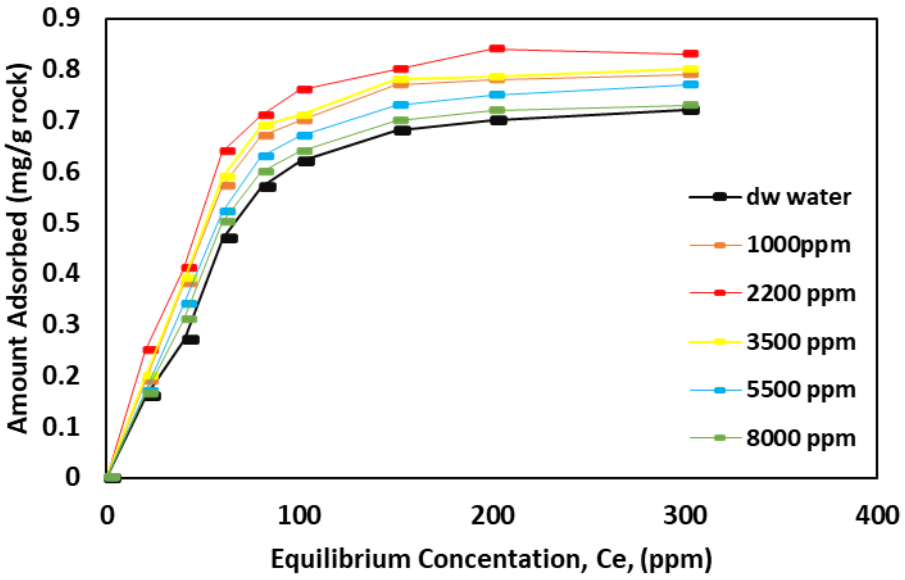

Figure 16. Single-component adsorption isotherms of Gemini surfactant T14S3 in deionised water and Na_2SO_4 media (1 000–8 000 ppm) at pH 8.0.

Nanosilica adsorption followed a different profile, with a more gradual rise and a higher plateau (~1.67 mg g^{-1} at 1300 ppm). The strong negative surface charge of nanosilica facilitates binding to positively charged calcite sites under the near-neutral pH 8.0 condition, likely involving hydrogen bonding between surface silanols and carbonate functional groups.

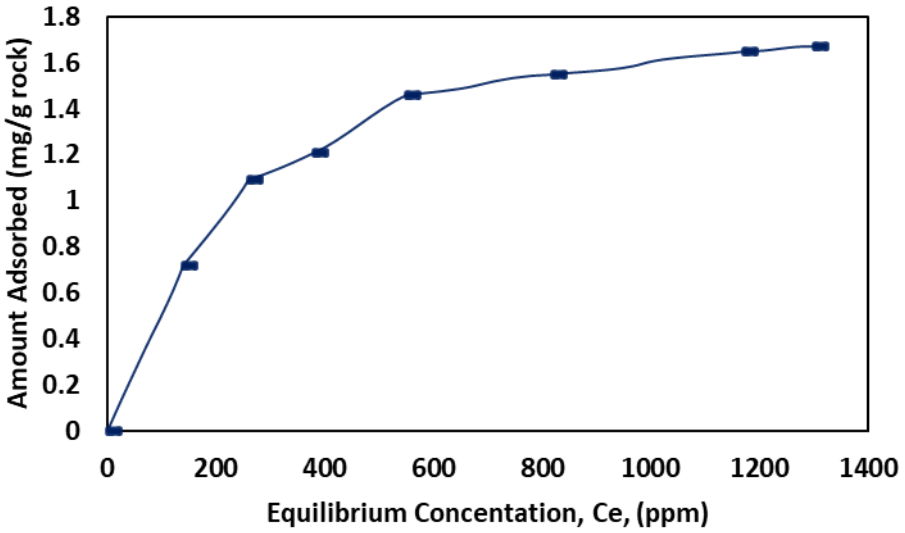

Figure 17. Single-component adsorption isotherm of green-derived nanosilica on carbonate rock at pH 8.0.

In the binary system containing 100 ppm GS and 550 ppm nanosilica, the total adsorption reached 2.30 mg/g rock (Table 9), composed of 0.70 mg/g GS and 1.60 mg/g nanosilica. Relative to single-component systems, GS adsorption increased by ~13% and nanosilica adsorption by ~9.6%. This mild positive synergy indicates that nanosilica serves as a carrier scaffold for GS, enabling co-deposition on the carbonate surface. Negatively charged nanosilica at pH 8 binds GS through electrostatic attraction, forming GS–nanosilica complexes that subsequently attach to rock surfaces, thereby bypassing direct site competition.

Introducing 2000 ppm Na_2SO_4 to the binary system maintained the total adsorption at 2.30 mg/g rock, but altered component distribution: 0.75 mg/g GS (+21%) and 1.55 mg/g nanosilica (6.1%). The Na^+ ions further compressed the double layer, allowing denser packing of GS molecules on both nanosilica particles and the carbonate substrate. SO_4^{2-} anions may facilitate counter-ion bridging between surfactant heads and Ca^{2+} surface sites.

In contrast, nanosilica adsorption decreased slightly, likely due to aggregation induced by electrolyte-mediated double-layer suppression, which reduces the available active surface area. Nevertheless, this loss is marginal and partly offset by the stabilisation of nanosilica–GS complexes at the interface.

Table 9. Synergistic adsorption of Gemini T14S3 and nanosilica in binary and ternary systems at pH 8.0

Fluid Formulation	Amount Adsorbed (mg/g)	GS (mg/g)	Nanosilica (mg/g)	Synergy Index (mg/g)
T14S3 GS+ Nanosilica	2.3	0.7	1.6	0.12
T14S3 GS+ Nanosilica+ Na2S04 salt	2.3	0.75	1.55	0.12

The equilibrium adsorption data of Gemini surfactant T14S3 and green-derived nanosilica on carbonate rock were analyzed using Langmuir and Freundlich isotherms, as shown in Figure 18.a

and Figure 18.b. For T14S3, the Langmuir model provided a good fit ($R^2 = 0.933$) with a monolayer capacity (q_m) of 0.946 mg g^{-1}, suggesting predominantly homogeneous site occupation. The Freundlich fit was less accurate ($R^2 = 0.823$), indicating limited multilayer or heterogeneous adsorption.

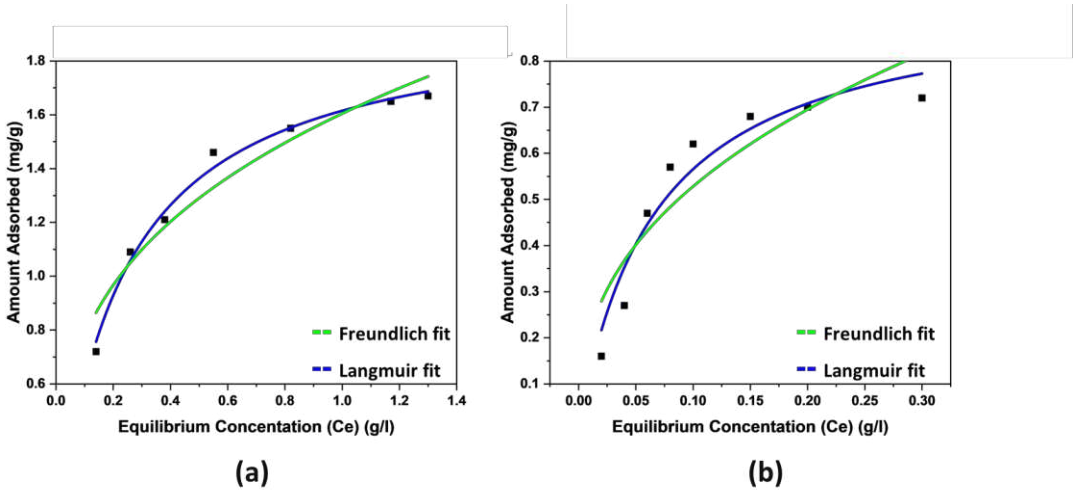

Figure 18. Langmuir and Freundlich adsorption isotherms for (a) Gemini surfactant T14S3 and (b) green-derived nanosilica on carbonate rock at pH 8.0.

In contrast, nanosilica exhibited a higher q_m of 1.98 mg g^{-1} with an outstanding Langmuir correlation ($R^2 = 0.9904$), reflecting strong interaction with carbonate surfaces, while the Freundlich parameters (n=3.18n = 3.18n=3.18, $R^2 = 0.933$) confirmed minor surface heterogeneity contributions. The fitted parameters and equations for both models are summarized in Table 10, supporting the conclusion that monolayer adsorption dominates for both adsorbates under the studied conditions.

Table 10. Fitted parameters, equations, and correlation coefficients (R^2) for Langmuir and Freundlich isotherm models applied to Gemini surfactant T14S3 and nanosilica adsorption.

	Model	Equation	Parameters	Isotherm Equation	R^2 Value
Gemini Surfactant (T14S3)	Langmuir isotherm	$q = \frac{q_m . k . C}{1 + k . C}$	q_m=0.946 k=14.85	$q = \frac{14.048C}{1 + 14.85C}$	R^2=0.933
	Freundlich isotherm	$q = k . C^{\frac{1}{n}}$	k=1.3142 n=2.526	$q = 1.314C^{0.3958}$	R^2=0.823

Nanosilica	Langmuir isotherm	$q = \frac{q_m . k . C}{1 + k . C}$	q_m=1.98 k=4.413	$q = \frac{8.73C}{1 + 4.413C}$	R^2=0.9904
	Freundlich isotherm	$q = k . C^{\frac{1}{n}}$	k=1.603 n=3.18	$q = 1.603C^{0.3144}$	R^2=0.93324

4-7 Spontaneous Imbibition Results

Figure 19 compares the cumulative oil recoveries of the three test scenarios after 60 days. The baseline brine (sea water salinity) yielded the lowest recovery, 12.4% OOIP, due to the mixed-wet to oil-wet character of the aged carbonate cores. In such systems, capillary forces oppose imbibition when the contact angle is high (>90°) and interfacial tension remains large, causing slow and incomplete oil displacement.

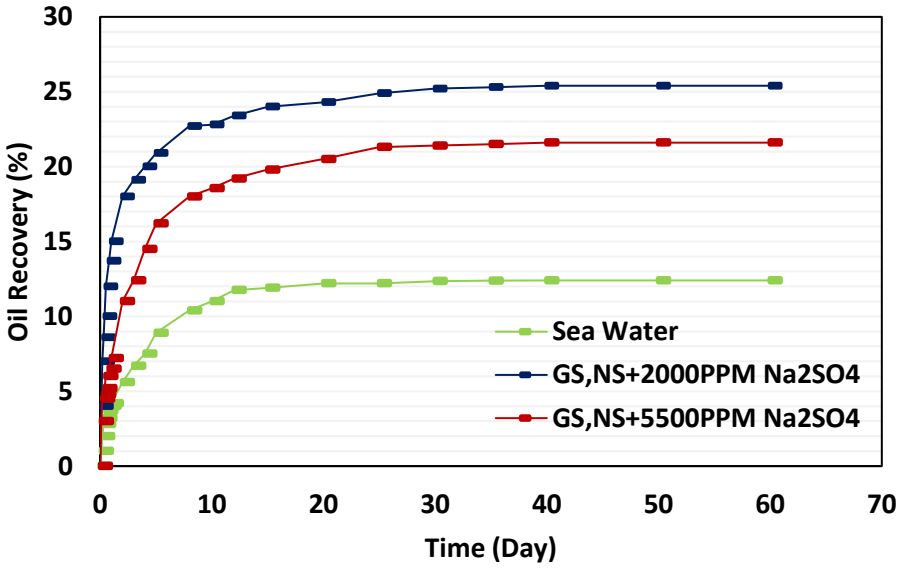

Figure 19 Oil recovery versus time during spontaneous imbibition tests for different fluid systems

In the optimized ternary formulation with 2000 ppm Na_2SO_4, ultimate recovery reached 25.4% OOIP, almost doubling the baseline value. This scenario corresponded to the most pronounced *wettability shift* towards a strongly water-wet state (contact angle reduction to the minimum observed in this work) while still providing substantial IFT reduction. The enhanced water-wetness increased the capillary pressure driving force ($Pc \propto \frac{\sigma cos\theta}{r}$) predominantly through the cosine term,

so that even moderate further reductions in IFT contributed proportionately less to the imbibition rate than the large change in cosθ. Mechanistically: (i) cationic Gemini T14S3 adsorbed strongly onto the carbonate surface by electrostatic attraction, neutralizing and then reversing surface charge at pH ≈ 8; (ii) nanosilica particles bridged surface asperities and delivered structural disjoining pressure, stabilizing the surfactant film; and (iii) moderate Na_2SO_4 concentration screened repulsive double-layer forces, maximizing molecular packing without destabilizing nanoparticles.

The high-salinity ternary system with 5500 ppm Na_2SO_4 produced 21.6% OOIP, outperforming the baseline but lagging behind the optimal salinity case. This salinity maximized *IFT reduction* (lowest measured σ) due to compression of the electrical double layer, increased surfactant adsorption at the oil–water interface, and possible micelle reorganization into more surface-active aggregates. However, the corresponding wettability alteration was less pronounced than in the 2000 ppm case, partly because high ionic strength fostered partial nanoparticle aggregation, reducing their ability to assist the surfactant in altering surface chemistry in smaller pores. With Pc scaling linearly with both σ and cosθ, these results suggest that in carbonates under static imbibition, a large increase in cosθ (wettability shift) exerts a more dominant impact on oil recovery than an equivalent percentage decrease in σ once IFT reaches the sub 1 mN/m range.

Taken together, these findings reveal that the governing mechanism for spontaneous imbibition in these carbonate cores is wettability alteration towards water-wetness, with IFT reduction playing a secondary, though synergistic, role. Achieving the right electrolyte concentration is therefore critical to balancing nanoparticle stability, surfactant adsorption at both the mineral and oil interfaces, and the relative weight of the two mechanisms, leading to optimal capillary-driven displacement.

5- Conclusion

This work demonstrates the successful integration of *Equisetum arvense*-derived nanosilica, a novel cationic Gemini surfactant (T14S3), and salinity tuning via Na_2SO_4 as a highly efficient, environmentally compatible EOR strategy for carbonate reservoirs. Structural characterization confirmed the amorphous, silanol-rich nature of the green nanosilica and the bis-quaternary, long-chain architecture of T14S3, both exhibiting adequate thermal stability for reservoir deployment.

Electrokinetic analyses revealed that nanosilica imparted strongly negative charges across the pH spectrum, promoting water wetness, whereas T14S3 maintained a high positive surface potential from acidic to alkaline conditions, favoring robust adsorption onto carbonate. Controlled Na_2SO_4 addition enabled precise modulation of the interfacial charge through divalent anion adsorption and electrical double-layer compression, providing charge tunability from strongly negative to strongly positive, depending on formulation.

The ternary system exhibited distinct optima for two key interfacial processes: the lowest IFT (0.51 mN/m) at 5500 ppm Na_2SO_4 and the most significant wettability alteration (final contact angle = 34°, from an initial ≈ 138°) at 2000 ppm Na_2SO_4. While the high-salinity condition maximized surfactant packing at the oil–water interface, moderate salinity preserved nanosilica dispersion stability and enhanced particle–surfactant cooperative adsorption on carbonate surfaces. Langmuir modeling confirmed monolayer adsorption for both components, with synergistic uptake in binary and ternary systems, further optimized under moderate ionic strength.

Spontaneous imbibition tests confirmed wettability alteration as the dominant recovery mechanism under the studied carbonate conditions. The optimized ternary formulation at 2000 ppm Na_2SO_4

achieved 25.4 % OOIP recovery, over twice the baseline brine case (12.4 %), while the 5500 ppm system yielded 21.6 % OOIP despite achieving the lowest IFT. These outcomes highlight that once IFT reaches the sub 1 mN/m regime, further reduction contributes less to imbibition than equivalent gains in water wetness ($\cos\theta$ effect). Thus, balancing electrolyte concentration to stabilize nanoparticles, enhance surfactant adsorption, and jointly optimize wettability and interfacial tension is critical for maximizing capillary-driven oil displacement.

Overall, this study establishes a mechanistically informed framework for coupling bio-derived nanoparticles, high-efficiency Gemini surfactants, and targeted salinity control. By uniting electrostatic tuning, hybrid interfacial film formation, and synergistic wettability reversal, this approach delivers both high technical performance and ecological compatibility, aligning with circular economy principles for future sustainable EOR operations.

6- Declarations

6-1 Data Availability Statement

All data will be available on academic request from the corresponding author.

6-2 Competing Interest

The authors declare that they have no conflict of interest.

6-3 Funding

The authors declare that no funds, grants, or other support were received during the preparation of this manuscript.

7- Author Contributions

- **Ali Yarahmadi:** Conceptualization; Writing – original draft; Data analysis; Experimental work.
- **Ghasem Zargar:** Supervision; Writing – review & editing.

- **Siavash Ashoori:** Supervision; Data validation.
- **Abbas Khaksar Manshad:** Supervision; Writing – review & editing.

References

1. Lakatos, I. and J. Lakatos-Szabo, *Global oil demand and role of chemical EOR methods in the 21st century.* International Journal of Oil, Gas and Coal Technology, 2008. **1**(1-2): p. 46–64.
2. Manrique, E., et al. *EOR: current status and opportunities*. in *SPE Improved Oil Recovery Conference?* 2010. SPE.
3. Joshi, R.M. and K.H. Singh, *Carbonate reservoirs: Recent large to giant carbonate discoveries around the world and how they are shaping the carbonate reservoir landscape*, in *Petro-physics and Rock Physics of Carbonate Reservoirs: Likely Elucidations and Way Forward*. 2019, Springer. p. 3–14.
4. Altunina, L., et al. *Advanced compositions for increasing oil recovery on the principles of "green chemistry"*. in *AIP Conference Proceedings*. 2022. AIP Publishing LLC.
5. Jiang, K., et al., *Nanomaterials in EOR: a review and future perspectives in unconventional reservoirs.* Energy & Fuels, 2023. **37**(14): p. 10045–10060.
6. Lakatos, I., G. Lakatos-Szabo, and G. Szentes. *Revival of green conformance and IOR/EOR technologies: nanosilica aided silicate systems-a review*. in *SPE International Conference and Exhibition on Formation Damage Control*. 2018. SPE.
7. Rahman, A., et al., *Nano-silica to reduce of surfactant adsorption in oil recovery: A review.* Environmental Chemistry Letters, 2025: p. 1–27.
8. Jumiati, W., et al., *Dynamic Adsorption and Oil Recovery of Nanosilica on Carbonate Rock.* ACS omega, 2024. **9**(44): p. 44134–44153.
9. Zamani, H., et al., *Biosynthesis of silica nanoparticle using Saccharomyces cervisiae and its application on enhanced oil recovery.* Journal of Petroleum Science and Engineering, 2020. **190**: p. 107002.
10. Javad Nazarahari, M., et al., *Synthesis, characterization, and assessment of a CeO2@ nanoclay nanocomposite for enhanced oil recovery.* Nanomaterials, 2020. **10**(11): p. 2280.

11. Manshad, A.K., et al., *Oil recovery aspects of ZnO/SiO2 nano-clay in carbonate reservoir.* Fuel, 2022. **307**: p. 121927.
12. Ali, J.A., et al., *Emerging applications of TiO2/SiO2/poly(acrylamide) nanocomposites within the engineered water EOR in carbonate reservoirs.* Journal of Molecular Liquids, 2021. **322**: p. 114943.
13. Nourinia, A., et al., *Synergistic Efficiency of Zinc Oxide/Montmorillonite Nanocomposites and a New Derived Saponin in Liquid/Liquid/Solid Interface-Included Systems: Application in Nanotechnology-Assisted Enhanced Oil Recovery.* ACS Omega, 2022. **7**(29): p. 24951–24972.
14. Bahraminejad, H., et al., *CuO/TiO2/PAM as a Novel Introduced Hybrid Agent for Water—Oil Interfacial Tension and Wettability Optimization in Chemical Enhanced Oil Recovery.* Energy & Fuels, 2019. **33**(11): p. 10547–10560.
15. Omidi, A., et al., *Smart- and nano-hybrid chemical EOR flooding using Fe3O4/eggshell nanocomposites.* Journal of Molecular Liquids, 2020. **316**: p. 113880.
16. Zargar, G., et al., *Experimental investigation of the effect of green TiO2/Quartz nanocomposite on interfacial tension reduction, wettability alteration, and oil recovery improvement.* Fuel, 2020. **263**: p. 116599.
17. Nazarahari, M.J., et al., *Impact of a novel biosynthesized nanocomposite (SiO2@Montmorilant@Xanthan) on wettability shift and interfacial tension: Applications for enhanced oil recovery.* Fuel, 2021. **298**: p. 120773.
18. Menger, F.M. and J.S. Keiper, *Gemini surfactants.* Angewandte Chemie International Edition, 2000. **39**(11): p. 1906–1920.
19. Kamal, M.S., *A review of gemini surfactants: potential application in enhanced oil recovery.* Journal of surfactants and detergents, 2016. **19**(2): p. 223–236.
20. Pal, N., N. Saxena, and A. Mandal, *Studies on the physicochemical properties of synthesized tailor-made gemini surfactants for application in enhanced oil recovery.* Journal of Molecular Liquids, 2018. **258**: p. 211–224.
21. Al-Azani, K., et al., *Synergistic performance of an in-house synthesized cationic Gemini surfactant for enhanced oil recovery under harsh conditions.* Fuel, 2024. **374**: p. 132359.

22. Wang, G., et al., *Cationic-anionic surfactant mixtures based on gemini surfactant as a candidate for enhanced oil recovery.* Colloids and Surfaces A: Physicochemical and Engineering Aspects, 2023. **677**: p. 132297.
23. Hou, B., et al., *A novel high temperature tolerant and high salinity resistant gemini surfactant for enhanced oil recovery.* Journal of Molecular Liquids, 2019. **296**: p. 112114.
24. Mpelwa, M., et al., *The study on the properties of the newly extended Gemini surfactants and their application potentials in the petroleum industry.* Journal of Petroleum Science and Engineering, 2020. **186**: p. 106799.
25. Yuan, T., et al., *Enhanced oil recovery from high-salinity reservoirs by cationic gemini surfactants.* Journal of Applied Polymer Science, 2018. **135**(14): p. 46086.
26. Ma, T., et al., *Property evaluation of synthesized anionic-nonionic gemini surfactants for chemical enhanced oil recovery.* Colloids and Surfaces A: Physicochemical and Engineering Aspects, 2019. **581**: p. 123800.
27. Chen, Z., et al., *Preparation and characterization of an anionic gemini surfactant for enhanced oil recovery in a hypersaline reservoir.* Journal of Surfactants and Detergents, 2019. **22**(6): p. 1309–1317.
28. Gu, Y., et al., *Preparation and performance evaluation of sulfate-quaternary ammonium Gemini surfactant.* Journal of Molecular Liquids, 2021. **343**: p. 117665.
29. Dong, Z., Y. Zheng, and J. Zhao, *Synthesis, Physico-Chemical Properties and Enhanced Oil Recovery Flooding Evaluation of Novel Zwitterionic Gemini Surfactants.* Journal of Surfactants and Detergents, 2014. **17**(6): p. 1213–1222.
30. Fattahi, R., et al., *Investigating the synergistic/antagonistic effects of mixing SiO2 nanoparticles and ionic liquid, nonionic emulsifier, and gemini surfactants on the main mechanisms of crude oil production.* Energy & Fuels, 2023. **37**(19): p. 14741–14751.
31. Turov, V. and R. Leboda, *Application of 1H NMR spectroscopy method for determination of characteristics of thin layers of water adsorbed on the surface of dispersed and porous adsorbents.* Advances in colloid and interface science, 1999. **79**(2-3): p. 173–211.